Science of the Total Environment 649 (2019) 1209–1223

Contents lists available at ScienceDirect

Science of the Total Environment

journal homepage: www.elsevier.com/locate/scitotenv

Cadmium accumulation capacity and resistance strategies of a cadmium-hypertolerant fern — *Microsorum fortunei*

Yun-Yun Yan, Bin Yang, Xin-Yu Lan, Xin-Yuan Li, Fu-Liu Xu *

MOE Laboratory for Earth Surface Processes, College of Urban & Environmental Sciences, Peking University, Beijing 100871, China

HIGHLIGHTS

- *Microsorum fortunei* could serve as a potential Cd-hypertolerant plant.
- *Microsorum fortunei* could sequester and detoxify most Cd in roots to protect the more Cd-sensitive leaves.
- Ribosome, catalytic activity and cellular process were the major GO terms identified for CC, MF and BP categories.
- *Microsorum fortunei* roots could resist Cd by antioxidants, plant hormones and other primary metabolites.

GRAPHICAL ABSTRACT

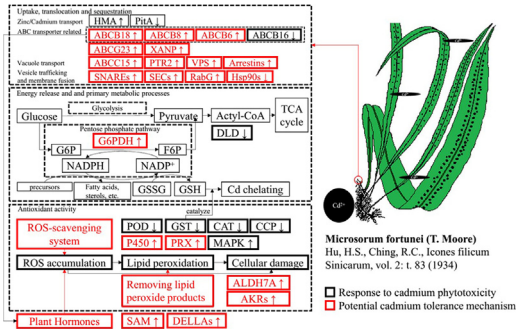

ARTICLE INFO

Article history:
Received 5 July 2018
Received in revised form 18 August 2018
Accepted 21 August 2018
Available online 23 August 2018

Editor: Jay Gan

Keywords:
Microsorum fortunei
Cadmium
Hypertolerant species
Transcriptome analysis

ABSTRACT

Microsorum fortunei (*M. fortunei*), a close relative to the cadmium (Cd) hyperaccumulator *Microsorum pteropus*, is an epiphytic Polypodiaceae fern with strong antioxidant activity. The Cd-accumulation capacities and Cd-resistance mechanisms of *M. fortunei* were analyzed in this study by measuring metal contents (Cd, Fe, Mg, Ca, Zn, Mn, K and Na) and chlorophyll fluorescence parameters (F_v/F_m, qN, qP, Y(II), Y(NPQ) and Y(NO)) and by performing an RNA-sequencing analysis. *M. fortunei* could accumulate up to 2249.10 μg/g DW Cd in roots under a 15-day 1000 μmol/L Cd treatment, with little Cd translocated into the leaves (maximum 138.26 μg/g DW). The *M. fortunei* leaves could maintain their normal physiological functions with no phytosynthesis damage and few changes in metal contents or differentially expressed genes. *M. fortunei* roots showed a decrease in Zn concentration, with potential Cd-tolerance mechanisms such as heavy metal transporters, vesicle trafficking and fusion proteins, antioxidant systems, and primary metabolites like plant hormones, revealed by differentially expressed functional genes. In conclusion, *M. fortunei* may serve as a potential cadmium-hypertolerant fern that sequesters and detoxifies most cadmium in the roots, with a minimum root-to-shoot Cd translocation to guarantee the physiological functions in the more vulnerable leaves.

1. Introduction

Cadmium (Cd) and its compounds, as Group 1 carcinogenic compounds (IARC, 1993), have become a worldwide environmental problem for their accumulation in soil and water, which would further cause toxic effects to humans in their lungs, kidneys, and skeletal and respiratory systems because of the long-term intake of Cd-contaminated food and drinking water (IARC, 1993; WHO, 2010). Phytoremediation is an effective in situ treatment to remove environmental heavy metals, and it heavily depends on hypertolerant species, or hyperaccumulators, that can both rapidly extract, sequester and tolerate 1,001,000-fold higher concentrations of heavy metals (100

* Corresponding author.
E-mail address: xufl@urban.pku.edu.cn (F.-L. Xu).

https://doi.org/10.1016/j.scitotenv.2018.08.281
0048-9697/

mg/kg·dry weight for cadmium) than those of non-hypertolerant plants (ITRC, 2010; Rascio and Navari-Izzo, 2011; Verbruggen et al., 2009b).

Both hyperaccumulators and hypertolerant species require special mechanisms to avoid phytotoxicity effects (Rascio and Navari-Izzo, 2011) and to phytoextract sufficient Cd, which can cause growth retardation, changes in metabolite contents, inhibition of photosynthesis and oxidative stress in plants, leading to further irreversible damage in organelles, membranes and even DNA (Basa et al., 2014; Kučera et al., 2008). The difference between hyperaccumulators and hypertolerant species mostly lies in their distribution of heavy metals. After the uptake of heavy metals in the rhizosphere, hyperaccumulators would rapidly translocate, effectively sequester and detoxify them in the aerial parts of the plant, while hypertolerant species mainly restrict and detoxify them in the roots, with minimized root-shoot translocation to protect the more vulnerable leaves (Baker et al., 1983; Rascio and Navari-Izzo, 2011).

Studies of Cd hyperaccumulators *Arabidopsis halleri* and *Thlaspi caerulescens* demonstrate that Cd influx/accumulation into plants is largely dependent on Zn transporters (Rascio and Navari-Izzo, 2011), such as ZNTs (zinc transporter). Other transporters, such as heavy metal ATPases (HMAs) (Takahashi et al., 2012), natural resistance-associated macrophage proteins (NRAMPs), Zinc-regulated transporter/iron-regulated transporter-like proteins (ZIPs), ATP-binding cassette (ABC) transporters, and yellow stripe 1-like proteins (YSLs), etc., also participate in cadmium transmembrane transport, from root uptake, vacuole sequestration to root-shoot translocation via the xylem (Feng et al., 2018; Saminathan et al., 2015). 'Sequestration' or 'compartmentalization' is a common detoxifying strategy to reduce the bioactivity of Cd^{2+} in plants (especially protoplasts), by transporting cadmium ions into nonsensitive regions, such as the trichome (Küpper et al., 2000), cuticle (Robinson et al., 2003), vacuole or apoplast (Clemens, 2006), and chelating them with amino acids, organic acids, metal-binding peptides and/or other ligands (Lan et al., 2018b; Rascio and Navari-Izzo, 2011). The antioxidant system is usually enhanced as a further defense mechanism to Cd-induced oxidative stress (Rascio and Navari-Izzo, 2011) in hypertolerant species with antioxidant enzymes, such as superoxide dismutase (SOD), peroxidase (POD), catalase (CAT), and glutathione reductase (GR), and non-enzymatic antioxidants, such as glutathione (GSH) (van de Mortel et al., 2008) and ascorbic acid (ASA) (Küpper et al., 1999), etc., while secondary metabolites and plant hormones also participate in this process.

M. fortunei, as a species in the genus *Microsorum* and family Polypodiaceae is a close relative to *Microsorum pteropus*, which has been proven to be a potential Cd hyperaccumulator (Lan et al., 2017; Lan et al., 2018b). Unlike the aquatic plant *Microsorum pteropus*, which usually grows on rocks and is fully or partially submerged in water according to the weather, *M. fortunei* is an epiphyte that grows on wet rocks in streams (Chen and Gilbert, 2006) in tropical and sub-tropical Asia. *M. fortunei* was studied to have a strong antioxidant activity and high total flavonoid content, with its ethanol extract maintaining a 96.11% scavenging rate of ABTS+ radicals (Li et al., 2011). Ferns are well known for their adaptations to extreme environments, attributed to their history of evolution in extreme habitats, such as the Cenozoic radiation of epiphytic ferns to accommodate an angiosperm-dominated canopy (Schuettpelz and Pryer, 2009). Ferns are also used as indicators to identify potential mine sites (Yoshihara et al., 2005). Little research has been conducted on hypertolerant mechanisms of ferns, except for *Athyrium yokoscense*, which accumulated a maximum of 3.3 mg/g·dry weight Cd in roots (without removing absorbed cadmium) in less than one month (Yoshihara et al., 2005). In this study, the Cd accumulation capacity, element content, leaf physiological indexes, and the transcriptome profile of *M. fortunei* were analyzed to evaluate its potential to accumulate and detoxify Cd.

2. Materials and methods

2.1. Plant materials and cadmium treatment

M. fortunei adult plants, with a length of approximately 60 cm, were collected in the Dujiangyan Conservation Area. The *M. fortunei* samples were partly submerged into 250 mL 10% Hoagland solution (pH = 6.0) with the leaves (fronds and stipes) above the solution and were precultured for 7 days. Then, the samples were exposed to 0, 50, 500, and 1000 μmol/L Cd^{2+} for 15 days. Both the plant cultivation and cadmium exposure procedures were conducted in an RXZ intelligent artificial climate box with 90% humidity, a temperature of 17 °C, and a 9 h light/15 h dark photoperiod under 3300 lx fluorescent lights.

After exposure, the *M. fortunei* samples were separated into roots (roots and rhizomes) and leaves (fronds and stipes). Fresh leaves were used to determine the chlorophyll fluorescence parameters (see Section 2.2), while the roots were immersed in 40 mL 0.01 mol/L EDTA-Na_2 solution for 2 h in order to remove the metals absorbed on the root surface. Both the leaves and roots were washed three times with deionized water, dried with absorbent paper and stored at −20 °C.

2.2. Determination of chlorophyll fluorescence parameters

After a 20-min dark adaption, fresh *M. fortunei* fronds were placed into a Maxi-Imaging-PAM chlorophyll fluorometer (Walz, Germany, 2005) to determine the chlorophyll fluorescence parameters, including F_m (maximal fluorescence yield in a dark-adapted state, with all PS II centers open), F_o (minimal fluorescence yield in a dark-adapted state, with all PS II centers open), qN (non-photochemical quenching coefficient), qP (photochemical quenching coefficient), Y(NPQ) (quantum yield of light-induced non-photochemical quenching, or quantum yield of regulated thermal dissipation in PS II) and Y(II) (effective quantum yield of PS II). The values for F_v/F_m (maximum efficiency of photosystem II) and Y(NO) (quantum yield of non-regulated thermal dissipation in PSII) were calculated according to the following formulas (Gallego et al., 2012; Klughammer and Schreiber, 2008):

$$F_v = F_m - F_o$$

$$Y(NO) + Y(NPQ) + Y(II) = 1$$

2.3. Determination of metal concentration

The treated leaves and roots were freeze-dried (Eyela FDU-830) for 72 h, weighed, and digested with 10 mL concentrated HNO_3 in quartz digestion tubes by a Digi Block ST36 digester (LabTech, Beijing, China) at 90 °C for 30 min, then at 160 °C for approximately 5 h until the digested products turned clear and colorless. The residual liquid was diluted with 5% HNO_3 to 25 mL, filtered through a 0.45-μm polyether sulfone filter, and measured in an inductively coupled plasma spectrometer (ICP-OES; Optima 5300DV, Institute of Geographic Sciences and Natural Resources Research, CAS). The bioconcentration factor (BCF) was calculated according to the following formula (Arnot and Gobas, 2006):

$$BCF = \frac{C_B\ (\text{Chemical concentration in the organism})}{C_{WD}\ (\text{Chemical concentration in water})}$$

2.4. RNA extraction and RNA-seq analysis

For the control and 1000 μmol/L Cd^{2+} exposed group, the RNA was extracted from the *M. fortunei* roots and leaves from the three biological replicates by an RNeasy Mini Kit (Qiagen, Germany). The cDNA library was prepared by Illumina kits, then sequenced by an Illumina HiSeq

2000 platform (Illumina, Inc., US). The quality assessment of the raw reads was conducted on FastQC v.0.10.1 (http://www.bioinformatics.babraham.ac.uk). The 487, 667 transcripts were assembled by Trinity v2.4.0 (Grabherr et al., 2011), which were further clustered with a 95% threshold to remove the redundant sequences by Cd-hit v4.6.8 (Fu et al., 2012; Li and Godzik, 2006), with 389,608 transcripts retained.

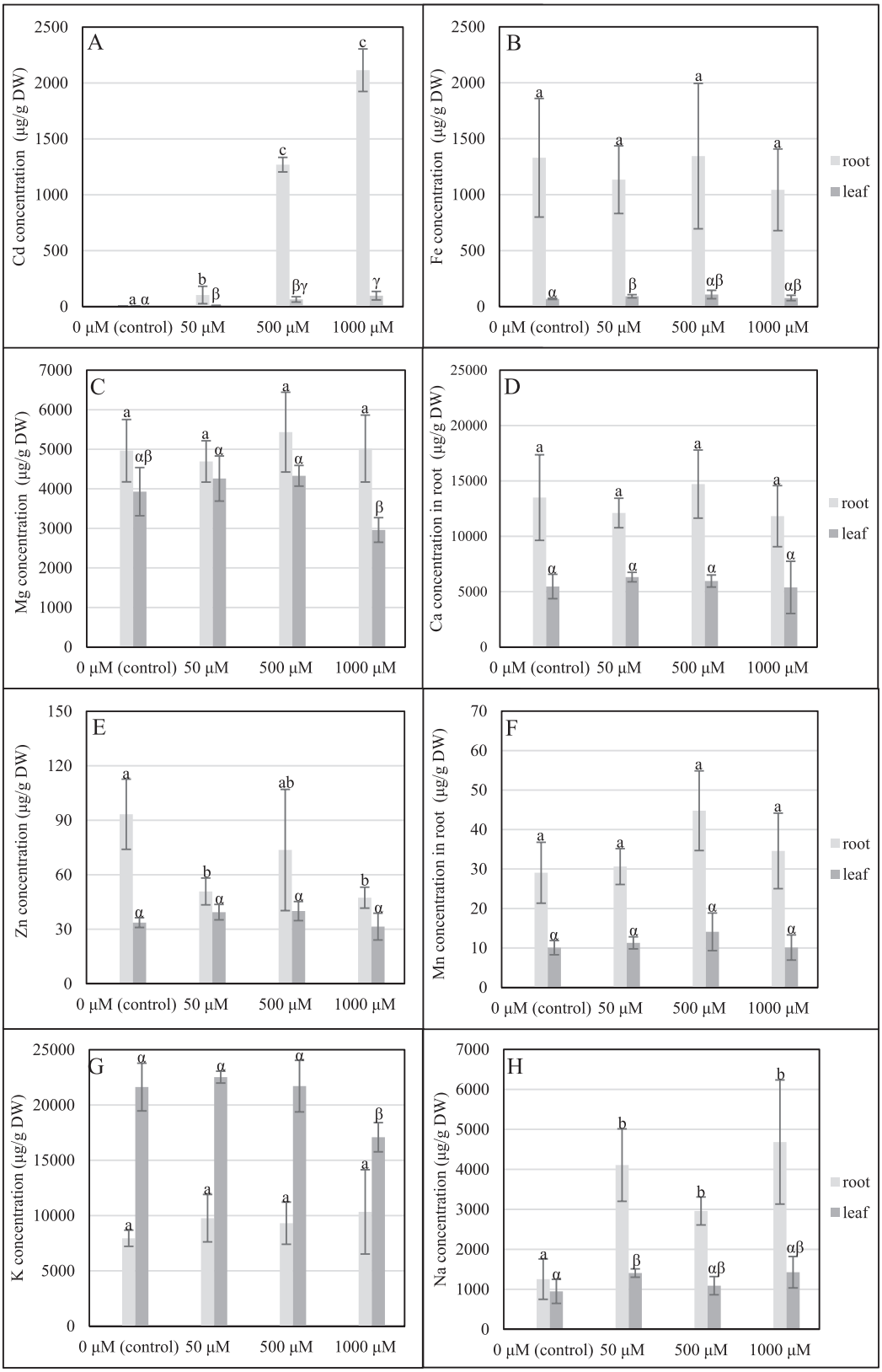

Fig. 1. The concentration of cadmium (Cd, A), iron (Fe, B), magnesium (Mg, C), calcium (Ca, D), zinc (Zn, E), manganese (Mn, F), potassium (K, G) and sodium (Na, H) in *M. fortunei* under the 0, 50, 500 and 1000 μmol/L Cd^{2+} exposure. The mean ± SD from three biological replicates was used, while treatment groups with a significant difference ($p < 0.05$) between their values are shown by different letters.

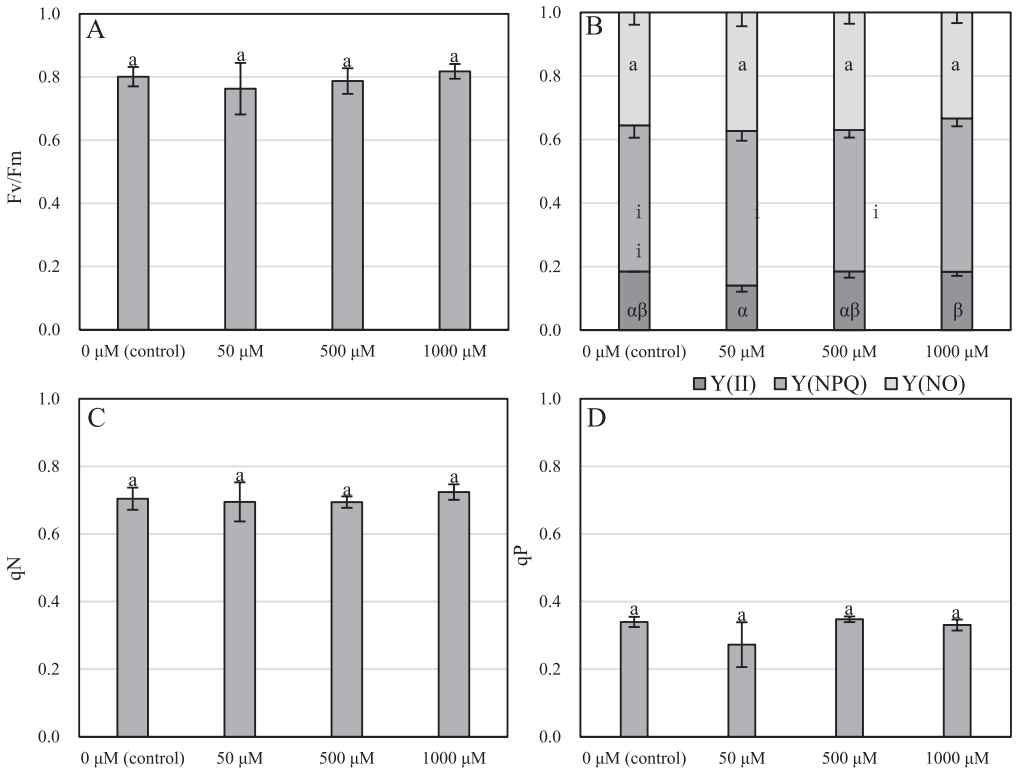

Fig. 2. Changes in chlorophyll fluorescence parameters induced by 0, 50, 500 and 1000 μmol/L Cd^{2+} exposure in *M. fortunei*, including (A) maximum efficiency of photosystem II (F_v/F_m), (B) effective quantum yield of photosystem II (Y(II)), quantum yield of regulated thermal dissipation in photosystem II (Y(NPQ)), and quantum yield of non-regulated thermal dissipation in photosystem II (Y(NO)), (C) non-photochemical quenching coefficient (qN) and (D) photochemical quenching coefficient (qP). The mean ± SD from three biological replicates was used, while treatment groups with a significant difference ($p < 0.05$) between their values are shown by different letters.

The transcripts were annotated by Diamond v0.8.22.84 (Buchfink et al., 2015) with gene ontology (GO) terms, for which the NCBI nr protein database was searched with a Blast cutoff e-value of 1×10^{-5}. To estimate the abundance in 12 samples (control and 1000 μmol/L Cd exposure group × 2 organisms × 3 replicates), sequence reads for each sample were aligned to the Trinity-assembled transcript sequences by RSEM v1.2.8 (Li and Dewey, 2011) using default parameters, with Bowtie 1.1.2 (Langmead et al., 2009) used for reference preparation and Samtools v1.3.1 (Li et al., 2009) called for the expression calculation. The expression estimates from all samples were combined into a matrix. The matrix was analyzed for the differential expression by the down-stream functions of Trinity v2.4.0 (Grabherr et al., 2011), which used the edgeR package (Chen et al., 2014) in R v3.2.0, and called additional files to indicate the biological replicate relationships in treatment groups. After the TMM normalization, differentially expressed genes with FDR < 0.001 and $\log_2$ (Fold Change) > 2 were listed, which were further clustered by DAVID (Huang et al., 2008) and PANTHER (Mi et al., 2009; Thomas et al., 2003).

2.5. Statistical analysis

At least three biological replicates were used for all experiments. With the SPSS 22.0 software package (Chicago, Illinois, USA), an ANOVA with Tukey's test or Games-Howell's test was used for statistical analysis, while an independent samples *t*-test was conducted for the significance test between the different treatment groups at a 0.05 probability level.

3. Results

3.1. Metal concentration

M. fortunei accumulated cadmium up to 2249.10 μg/g DW in the roots and 138.26 μg/g DW in the leaves under 1000 μmol/L Cd^{2+} exposure. The Cd concentration in the roots significantly ($p < 0.05$) rose with the increasing Cd^{2+} treatment, although no significant difference was found between plants under 500 and 1000 μmol/L Cd^{2+} exposure ($p > 0.05$). The Cd content in leaves exposed to Cd^{2+} had a significant increase ($p < 0.05$) compared with that in the control group, while no significant difference was found among *M. fortunei* leaves under 50 to 1000 μmol/L Cd^{2+} application except for the leaves under 50 and 1000 μmol/L Cd^{2+} exposure ($p < 0.05$) (Fig. 1A). Under exposure to 50, 500 and 1000 μmol/L Cd^{2+}, the bioaccumulation factor (BCF) for *M. fortunei* was 18.35, 22.58, 18.81 for the roots, and 1.45, 1.14, 0.87 for the leaves, respectively. Moreover, the shoot/root ratio of the Cd concentration had an average value of 0.05, with no significant difference found among the different Cd^{2+} treatment groups ($p > 0.05$).

Meanwhile, the concentrations of Fe (Fig. 1B), Mg (Fig. 1C), Ca (Fig. 1D), Zn (Fig. 1E), Mn (Fig. 1F), K (Fig. 1G) and Na (Fig. 1H) were measured for their potential roles in Cd uptake, transport, as well as resistance to Cd toxicity. Compared with the control group, no significant difference ($p > 0.05$) was observed for the concentration of Fe, Mg, Ca and Mn in Cd-exposed roots and leaves, except for a slight increase in Fe content of the 50 μmol/L Cd^{2+} exposed leaves ($p < 0.05$). Compared with the control, the root Zn concentration decreased under Cd^{2+} exposure (significantly ($p < 0.05$) under the 50 or 1000 μmol/L Cd^{2+} exposure), while no significant difference was found for the leaf Zn concentration. The K concentration decreased significantly ($p < 0.05$) in *M. fortunei* leaves under the 1000 μmol/L Cd^{2+} treatment, while no significant difference ($p > 0.05$) was observed for the other exposure groups in the leaves and roots. Compared with the control group, the Na concentration in the *M. fortunei* roots increased significantly ($p < 0.05$) after the application of 50–1000 μmol/L Cd^{2+}, while the Na content in the leaves also increased under Cd^{2+} exposure, with a significant difference only observed for the 50 μmol/L Cd^{2+} treatment group.

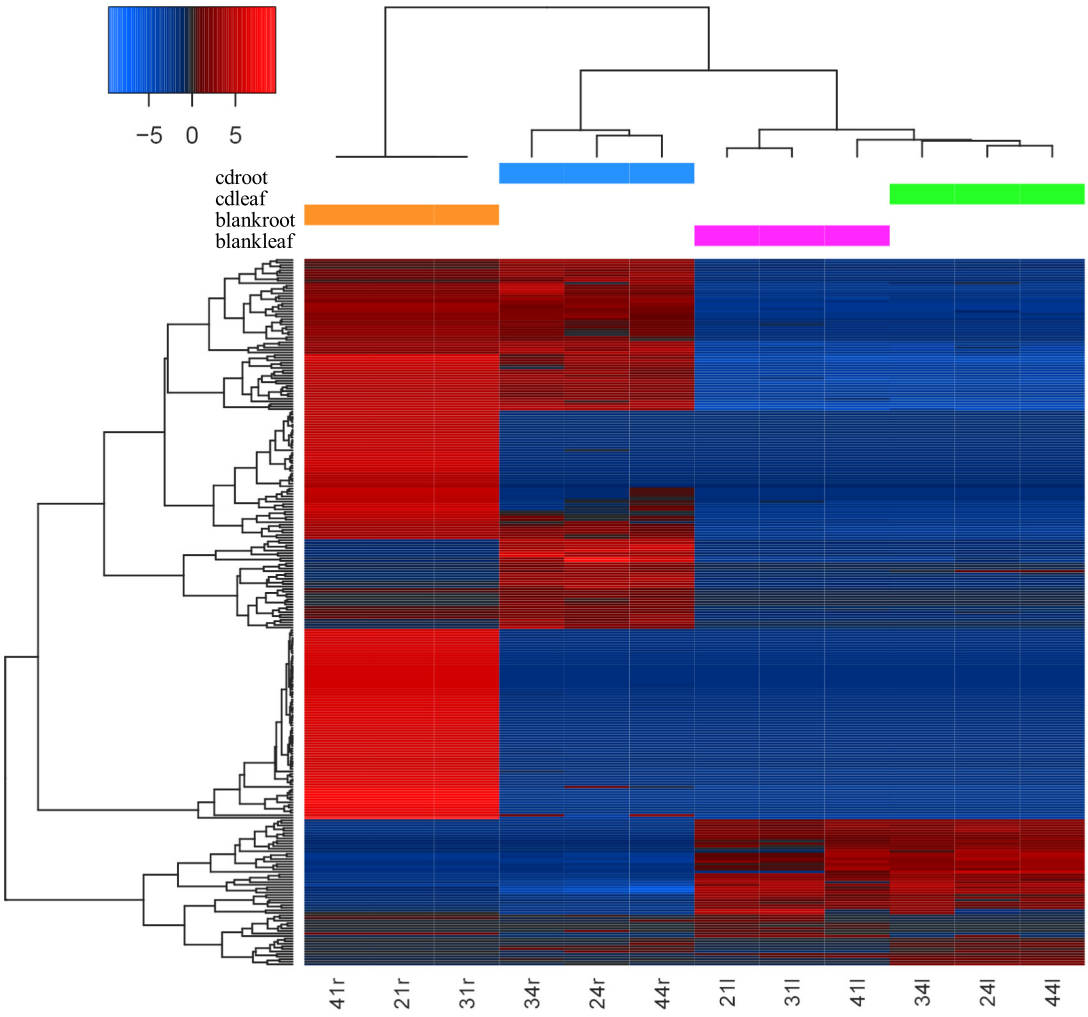

Fig. 3. Heatmap of differentially expressed (DE) genes with clusters in *M. fortunei*. The top 100 of the DE features within each pairwise comparison, namely, a total number of 276 genes, were extracted. The value of the color key is defined as $\log_2$(FPKM (Fragments Per Kilobase Million) + 1) and was median-centered for normalization. Hierarchical cluster group marks, such as blankroot (or blankleaf) and cdroot (or cdleaf), represent the relevant organisms of the control group or 1000 μmol/L Cd^{2+} exposed group, respectively. The 276 genes were further clustered into six categories (listed on the left).

3.2. Chlorophyll fluorescence parameters

For the maximum efficiency of photosystem II (F_v/F_m) (Fig. 2A), the non-photochemical quenching coefficient (qN) (Fig. 2C) and the photochemical quenching coefficient (qP) (Fig. 2D) in the *M. fortunei* leaves, no significant difference ($p > 0.05$) was observed among the 0, 50, 500 and 1000 μmol/L Cd^{2+} treatment groups. Notably, for the effective quantum yield of photosystem II (Y(II)), the quantum yield of regulated (Y(NPQ)) and the non-regulated (Y(NO)) thermal dissipation in photosystem II, Y(NO) + Y(NPQ) + Y(II) = 1 (Fig. 2B). The Y(NPQ) is also known as the quantum yield of light-induced non-photochemical quenching, or an indicator of light-dependent ΔpH- and xanthophyll-mediated thermal dissipation in the PSII antennae (Gallego et al., 2012; Kalaji et al., 2017; Klughammer and Schreiber, 2008). For these three chlorophyll fluorescence parameters, no significant difference ($p > 0.05$) was found for *M. fortunei* leaves under Cd^{2+} exposure compared with the control group.

3.3. Transcriptome analysis

Comparing the three biological replicates of the control with those of the 1000 μmol/L Cd^{2+} treatment group, a total of 389,608 transcripts were identified. With FDR < 0.001 and $\log_2$(Fold Change) > 2, 18 differentially expressed transcripts were found between the blank group and the Cd exposed group in the leaves, while 108,950 were found for the roots (Fig. S1). The top 100 differentially expressed per comparison genes of the 12 samples (Fig. 3) indicated an obvious difference in transcriptome expression between the Cd-exposed roots and the blank roots, while little difference could be recognized between the differently treated leaves.

3.4. Functional classification analyses

For the 18 differentially expressed genes in the leaves, 10 genes were functionally annotated according to the NCBI nr database analysis by DAVID (Huang et al., 2008), and almost all the genes served for DNA or RNA activities (Table 1), except for a down-regulation of the PAH1-like phosphatidate phosphatase and an up-regulation of the MLO-like protein 10. The PAH1 is a magnesium-dependent phosphatidate phosphatase functioning at the endoplasmic reticulum (ER) that indirectly represses phospholipid biosynthesis along with PAH2, which affects the pathway of galactolipid synthesis and the mediate membrane lipid remodeling that serves as an essential adaptation mechanism for phosphate starvation (Eastmond et al., 2010; Mietkiewska et al., 2011; Nakamura et al., 2009). Meanwhile, MLO-like protein 10, with a GO-annotated biological process of defense response, may have a role in the modulation of pathogen defense and leaf cell death.

For the 108,950 differentially expressed genes in the roots under Cd treatment, 20,802 were functionally annotated by DAVID (Huang et al., 2008), with 17,910 down-regulated and 2892 up-regulated. *Physcomitrella patens* and *Selaginella moellendorffii* were selected as reference species, as close relatives to *M. fortunei*. Of these genes, 739 were annotated by *Physcomitrella patens*, with key regulated genes classified in precatalytic spliceosome, GTPase activity, proteolysis and vesicle fusion (Fig. 4A), while 540 were annotated by *Selaginella moellendorffii*, with a classification of GTPase activity, ribosome, cell wall, heme binding and oxidoreductase activity (Fig. 4B).

Furthermore, root differentially expressed genes annotated by *Physcomitrella patens* were clustered by the GO database analysis in PANTHER (Mi et al., 2009; Thomas et al., 2003). To better analyze the GO terms, the parent-child relationship ("is_a" or "part_of") between the GO terms was considered. For the cellular component category (Fig. 5A), cell part, organelle, macromolecular complex and membrane were the primary presented parent terms, with 311, 209, 146 and 41 gene counts differentially expressed, respectively. The intracellular and cytoplasm terms, as child GO terms to cell part, had much higher gene counts of 286 and 220, respectively, than that of the organelle. For the molecular function category (Fig. 5B), the catalytic activity, binding, structural molecule activity and transporter activity composed the parent terms, with gene counts of 206, 137, 67 and 51, respectively. In terms of the biological process category (Fig. 5C), cellular process, metabolic process, cellular component organization or biogenesis, localization, biological regulation and response to stimulus were the identified parent terms with 308, 289, 93, 61, 61 and 54 gene counts, respectively.

In addition to the gene counts, the expression pattern of each GO term was characterized by the z-score and adjusted p-value, to render the false discovery rate (FDR) and the up/down-regulation scales of each clustered GO term, respectively. Note that the bubbles (Fig. 5D) with a high $-\log_{10}$(adj. p-value) value were also those with high gene counts, except for the molecular function category in which the structural constituent of ribosome (61 counts), structural molecule activity (67 counts), catalytic activity (210 counts), and binding (138 counts), in order, were the top 4 for the $-\log_{10}$(adj. p-value). For the cellular component, the top three for $-\log_{10}$(adj. p-value) were cell part, intracellular, and cytoplasm. For the biological process, the cellular process had the maximum $-\log_{10}$(adj. p-value), while metabolic process and its child terms were ranked 2nd to 5th. For the bars arranged according to the z-score (Fig. 5E), the structural molecule activity (MF), structural constituent of ribosome (MF), ribosome (CC), ribonucleoprotein complex (CC) and cytosol (CC) was observed to have a superior proportion of down-regulated genes, while the transferase activity (MF) was the GO term with the highest proportion of up-regulated genes.

The detailed functions and potential detoxification mechanisms of *M. fortunei* under Cd stress are further analyzed in Section 4, the Discussion.

4. Discussion

According to the results, *M. fortunei* roots and leaves behaved quite differently under cadmium stress. *M. fortunei* roots accumulated up to 2249.10 μg/g DW Cd, maintained a high BCF, and genes transcript levels were highly differentially expressed. By contrast, *M. fortunei* leaves had <1/10 the cadmium content and BCF value compared with those of roots, with little photosynthetic damage, mineral concentration changes or differentially expressed transcripts, even under 1000 μM Cd^{2+} exposure. Considering the less-than-one S/R ratio and a decreasing BCF in the leaves under increasing Cd^{2+} exposure, *M. fortunei* may serve as a cadmium-hypertolerant plant (Rascio and Navari-Izzo, 2011), which has a mechanism of storing and detoxifying most of the cadmium in the roots, with a minimized root-to-shoot cadmium transport to avoid the phytotoxic effects in the leaves.

With a Cd concentration much higher than the proposed 100 mg/kg DW threshold level of Cd hyperaccumulators (Verbruggen et al., 2009b), *M. fortunei* could be applied for the remediation of Cd-contaminated water or soil. The potential mechanisms of detoxification in the roots are discussed below, although all of these mechanisms require further verification by q-PCR and protein analysis.

4.1. Expression patterns of 9 GO terms and relevant genes

To better analyze the differentially expressed functional genes related to cadmium tolerance, genes relevant to 9 gene ontology (GO) terms were graphically represented by the R package GOplot (Walter et al., 2015). For each GO term, an overall upward/downward

Table 1
Differentially expressed genes in leaves annotated by DAVID.

Gene symbol	Gene description	Log FC	Gene ontology (GO) terms			Reference species
			Biological process	Cellular component	Molecular function	
PHYPADRAFT_170225	Hypothetical protein	−8.93	RNA export from nucleus, protein import into nucleus	Nuclear pore inner ring	Structural constituent of nuclear pore	*Physcomitrella patens*
PHYPADRAFT_7275	Hypothetical protein	−9.93	–	Nucleus	DNA binding	*Physcomitrella patens*
PHYPADRAFT_183414	Hypothetical protein	−10.18	DNA repair, histone acetylation	Histone acetyltransferase complex, nucleus	Kinase activity	*Physcomitrella patens*
LOC106319149	Phosphatidate phosphatase PAH1-like	−10.01	–	–	–	*Brassica oleracea*
PHYPADRAFT_91582	Hypothetical protein	9.06	RNA processing	Nucleus, cytoplasm	ATP-dependent RNA helicase activity, ATP binding, poly(A) RNA binding	*Physcomitrella patens*
SELMODRAFT_125741	Hypothetical protein	10.24	–	Integral component of membrane	–	*Selaginella moellendorffii*
SELMODRAFT_169248	Hypothetical protein	5.59	–	Integral component of membrane	–	*Selaginella moellendorffii*
LOC102622193	Hypothetical protein	10.12	Carbohydrate metabolic process, pentose-phosphate shunt	Cytoplasm	Sedoheptulose-7-phosphate: D-glyceraldehyde-3-phosphate glyceronetransferase activity	*Citrus sinensis*
LOC108214317	Probable RNA-dependent RNA polymerase 3	9.14	–	–	RNA-directed RNA polymerase activity	*Daucus carota* subsp. *sativus*
LOC100233061	MLO-like protein 10	9.53	Defense response, response to biotic stimulus	Plasma membrane, integral component of membrane		*Vitis vinifera*

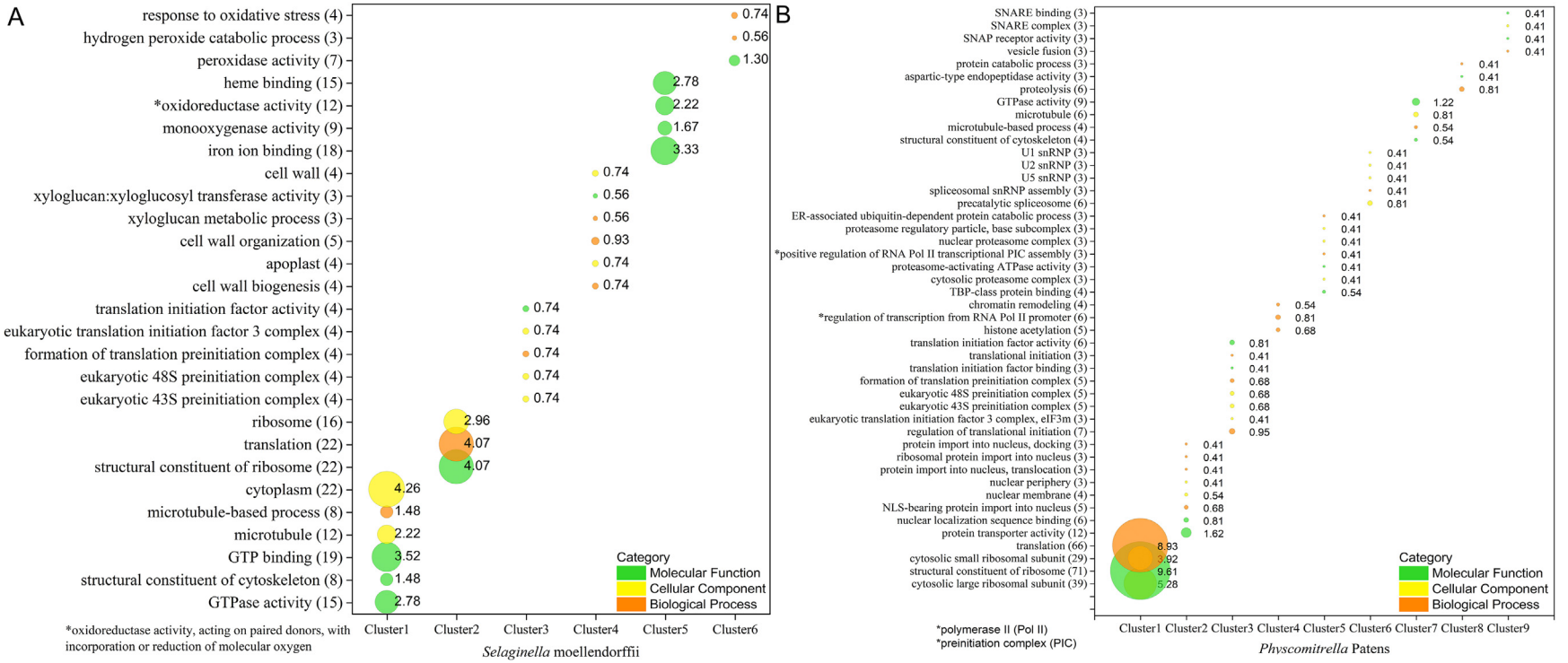

Fig. 4. Differentially expressed genes in *M. fortunei* roots annotated by *Physcomitrella patens* (A) and *Selaginella moellendorffii* (B) by NCBI nr database analysis in DAVID (Huang et al., 2008). Each GO functional term is listed with expressed gene counts in brackets. The color of the bubbles was defined by their GO category. The size of the bubbles were defined by the gene ratio (%) listed beside the bubbles, which is the ratio between the expressed gene counts of the GO term and the total gene counts in that GO category. (For interpretation of the references to color in this figure legend, the reader is referred to the web version of this article.)

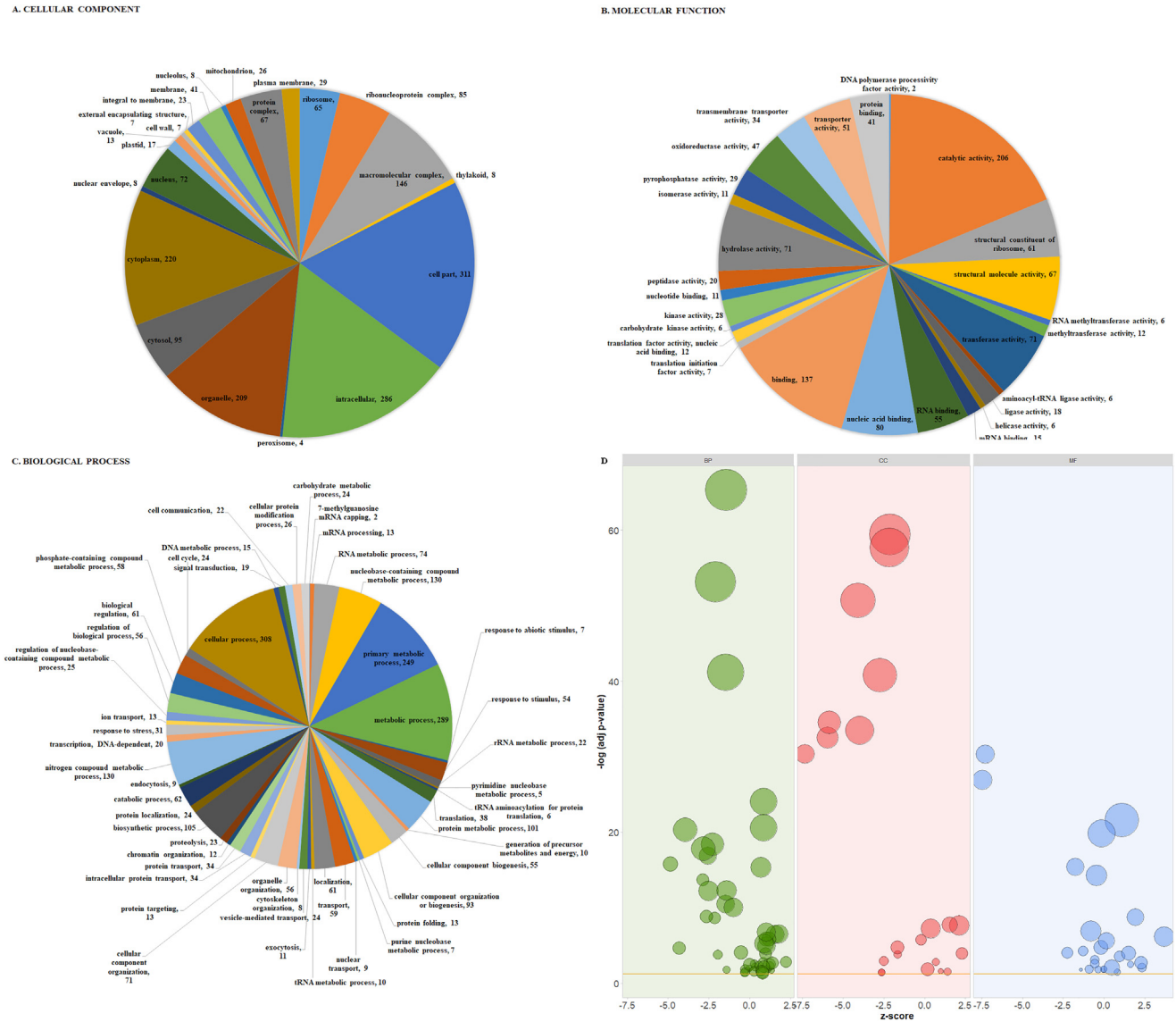
A. CELLULAR COMPONENT
nucleolus, 8
mitochondrion, 26
plasma membrane, 29
membrane, 41
integral to membrane, 23
external encapsulating structure, 7
cell wall, 7
vacuole, 13
plastid, 17
nuclear envelope, 3
nucleus, 72
cytoplasm, 220
cytosol, 95
organelle, 209
peroxisome, 4
intracellular, 286
cell part, 311
thylakoid, 8
macromolecular complex, 146
ribonucleoprotein complex, 85
ribosome, 65
protein complex, 67
B. MOLECULAR FUNCTION
DNA polymerase processivity factor activity, 2
protein binding, 41
transporter activity, 51
transmembrane transporter activity, 34
oxidoreductase activity, 47
pyrophosphatase activity, 29
isomerase activity, 11
hydrolase activity, 71
peptidase activity, 20
nucleotide binding, 11
kinase activity, 28
carbohydrate kinase activity, 6
translation factor activity, nucleic acid binding, 12
translation initiation factor activity, 7
binding, 137
nucleic acid binding, 80
RNA binding, 55
catalytic activity, 206
structural constituent of ribosome, 61
structural molecule activity, 67
RNA methyltransferase activity, 6
methyltransferase activity, 12
transferase activity, 71
aminoacyl-tRNA ligase activity, 6
ligase activity, 18
helicase activity, 6
C. BIOLOGICAL PROCESS
carbohydrate metabolic process, 24
cell communication, 22
cellular protein modification process, 26
7-methylguanosine mRNA capping, 2
mRNA processing, 13
DNA metabolic process, 15
cell cycle, 24
signal transduction, 19
RNA metabolic process, 74
phosphate-containing compound metabolic process, 58
nucleobase-containing compound metabolic process, 130
biological regulation, 61
regulation of biological process, 56
regulation of nucleobase-containing compound metabolic process, 25
cellular process, 308
response to abiotic stimulus, 7
primary metabolic process, 249
response to stimulus, 54
metabolic process, 289
rRNA metabolic process, 22
ion transport, 13
response to stress, 31
transcription, DNA-dependent, 20
nitrogen compound metabolic process, 130
pyrimidine nucleobase metabolic process, 5
endocytosis, 9
catabolic process, 62
tRNA aminoacylation for protein translation, 6
protein localization, 24
translation, 38
biosynthetic process, 105
protein metabolic process, 101
proteolysis, 23
generation of precursor metabolites and energy, 10
chromatin organization, 12
protein transport, 34
cellular component biogenesis, 55
intracellular protein transport, 34
organelle organization, 56
localization, 61
cytoskeleton organization, 8
transport, 59
cellular component organization or biogenesis, 93
protein targeting, 13
vesicle-mediated transport, 24
protein folding, 13
exocytosis, 11
purine nucleobase metabolic process, 7
cellular component organization, 71
nuclear transport, 9
tRNA metabolic process, 10
D
BP
CC
MF
-log (fdj p-value)
z-score
E
BP
CC
MF
Z-score
decreasing
increasing
-log (fdj p-value)
transcription, DNA-dependent
localization
transport
*metabolic process
regulation of nucleobase-containing compound mp*
pyrimidine nucleobase metabolic process
vesicle-mediated transport
protein transport
purine nucleobase metabolic process
regulation of biological process
phosphate-containing compound metabolic process
intracellular protein transport
protein localization
biological regulation
nucleobase-containing compound metabolic process
cell communication
protein targeting
carbohydrate metabolic process
cellular protein modification process
RNA metabolic process
signal transduction
chromatin organization
nuclear transport
cell cycle
DNA metabolic process
response to stress
endocytosis
mRNA processing
ion transport
7-methylguanosine mRNA capping
tRNA aminoacylation for protein translation
cellular component organization
cellular process
primary metabolic process
organelle organization
protein folding
metabolic process
rRNA metabolic process
cellular component organization or biogenesis
proteolysis
protein metabolic process
response to abiotic stimulus
biosynthetic process
generation of precursor metabolites and energy
cellular component biogenesis
translation
integral to membrane
nucleus
membrane
peroxisome
nucleolus
nuclear envelope
plasma membrane
plastid
thylakoid
mitochondrion
cell part
intracellular
vacuole
external encapsulating structure
cell wall
organelle
macromolecular complex
cytoplasm
cytosol
ribonucleoprotein complex
ribosome
transferase activity
methyltransferase activity
kinase activity
RNA methyltransferase activity
transporter activity
transmembrane transporter activity
catalytic activity
ligase activity
carbohydrate kinase activity
helicase activity
oxidoreductase activity
peptidase activity
aminoacyl-tRNA ligase activity
binding
pyrophosphatase activity
translation initiation factor activity
nucleotide binding
nucleic acid binding
hydrolase activity
isomerase activity
DNA polymerase processivity factor activity
mRNA binding
RNA binding
peptidase activity
structural constituent of ribosome
structural molecule activity

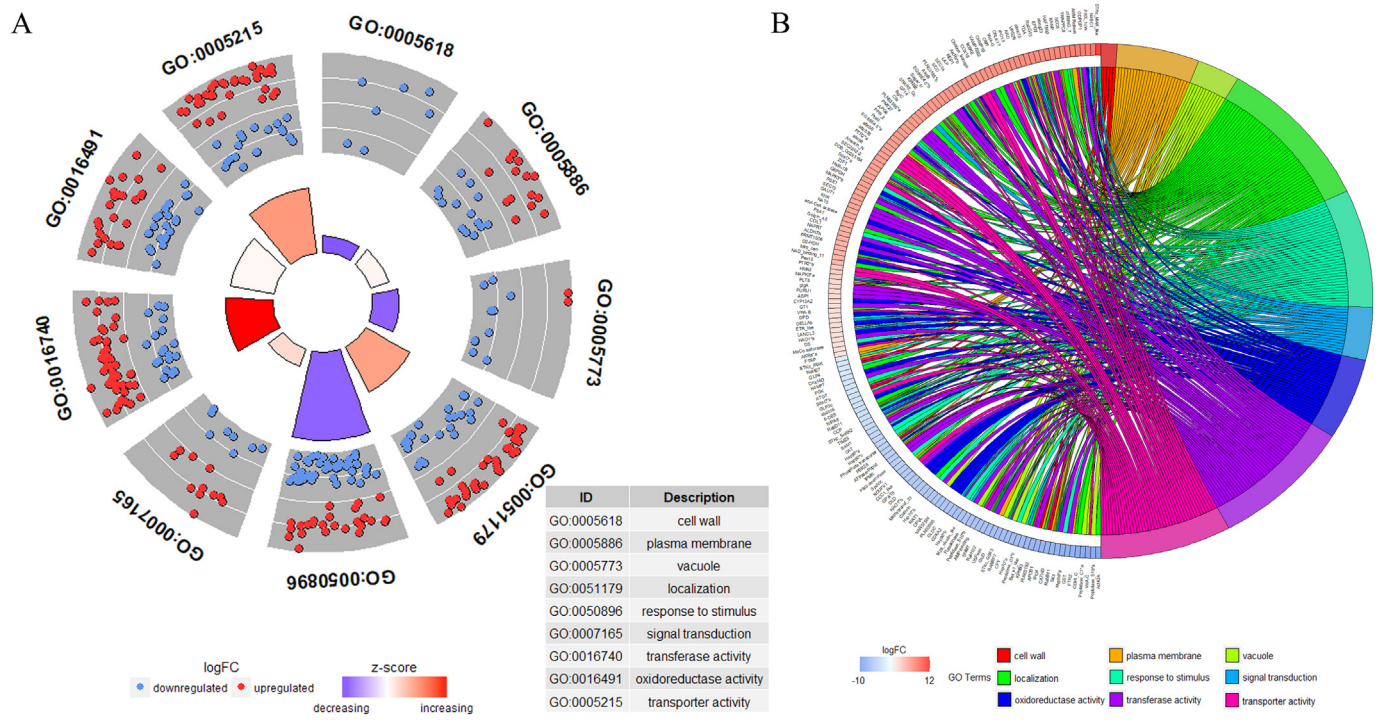

Fig. 6. Functional genes related to 9 gene ontology (GO) terms presented by GOplot (Walter et al., 2015). The 9 GO terms relevant to cadmium tolerance, from top to bottom and three by three, were from the cellular components (CC), biological processes (BP) and molecular functions (MF) categories, respectively. (A) The GOCircle plot displays the differential expression of 9 GO terms with 238 relevant genes. The outer ring indicates the gene expression level (logFC) for each GO term, with up-regulated (logFC > 0) or down-regulated (logFC < 0) genes categorized by the logFC color key. For the inner ring, the bar heights conduct as the term significance ($-\log_{10}$ adjusted p-value), and the bar colors represent the z-score. (B) The GOChord plot depicting genes linked to their assigned GO terms and ranked by their logFC. A total number of 163 genes (Table S1) were selected from the 238 genes after removing genes without specific functions or only related to DNA/RNA metabolites identified by PANTHER and NCBI. For the genes representing the same family protein, "*a", "*b", etc. was added for differentiation.

expression tendency (Fig. 6A) and the corresponding genes with specific functions (Fig. 6B) could be observed. For the overall expression pattern of each GO term according to the z-score, the gene expression of the cell wall (CC), vacuole (CC) and response to stimulus (BP) decreased evidently. The plasma membrane (CC), oxidoreductase activity (MF) and signal transduction (BP) were slightly up-regulated, while the localization (BP), transporter activity (MF) and transferase activity (MF) increased significantly. Specific genes with Cd-relevant functions are discussed below.

4.2. Heavy metal transporter activity

For the 34 genes identified with transmembrane transporter activity and the 51 genes identified with transporter activity in the Panther GO-Slim molecular function, 40 were selected and presented as relevant to heavy metal stress (Table 2).

The HMA2 (heavy metal transporting ATPase, HMA) was described to load Cd^{2+} into the xylem along with HMA4 (Mendoza-Cózatl et al., 2011; Verbruggen et al., 2009a); thus, the up-regulation of Cadmium/Zinc-Transporting ATPase HMA2-like in *M. fortunei* roots might indicate the mediating of the root-to-shoot translocation of Cd^{2+} under Cd exposure. Meanwhile, the pitA (inorganic phosphate transporter) in the PHO4 (phosphate transporter family) superfamily (Jackson et al., 2008; McCarthy et al., 2014) is an importer of alternative metals, such as Zn(II) in *Escherichia coli* (Beard et al., 2000), and was down-regulated in the *M. fortunei* roots. For the metal content, a significant decrease in Zn in the *M. fortunei* root was observed, while no Zn deficiency in the leaves was caused by the competition between Cd and Zn transport.

Six members of the ATP-binding cassette (ABC) transporter family were differentially expressed, with 5 up-regulated, except for ABCB16. In plants, ABCB and ABCG subfamily members (Geisler, 2014) have a role in phytohormones transport, such as auxins and abscisic acid (Geisler, 2014). As PGP/MDR group proteins (Çakır and Kılıçkaya, 2013), ABCB16 (Murphy et al., 2010) and ABCB18 may serve as auxin transporters at the plasma membrane. ABCG23 seems to have a plastidic-conserved function in non-photosynthetic tissues (Geisler, 2014) and co-expresses with non-plastidic transporters, such as AtABCG6, AtABCG20 and a xanthine/uracil permease family protein, At1g49960 (Geisler, 2014). Meanwhile, sequence identified as a xanthine permease family protein A9S4K1 was highly up-regulated in *M. fortunei*.

Moreover, the ABCC subfamily members are involved in vacuolar transport, which is related to cadmium tolerance in yeast (Çakır and Kılıçkaya, 2013). ABCC1/2, as the best-studied genes for the 15 recognized ABC subclass C transporters (ABCC1-15) in Arabidopsis, were believed to enhance cadmium sequestration in plant vacuoles by Cd-phytochelatin transport (Geisler, 2014; Mendoza-Cózatl et al., 2011), and the highly up-regulated ABCC15 might play a similar role in *M. fortunei*, although limited research on ABCC15 makes this role difficult to be verified.

Vacuolar-type H^+-ATPases (V-ATPases) are found to serve for Cd^{2+}/H^+ antiport activity in oat roots, which accumulate Cd^{2+} into tonoplast-

Fig. 5. Functional enrichment groups of three gene ontology (GO) categories: cellular component (A), molecular function (B) and biological process (C) in *M. fortunei*, with the expression pattern of each GO term presented by GOBubble (D) and GOBar (E) (Walter et al., 2015). The GO terms and expressed gene counts are listed on each part of the pie chart (A, B, C). The z-scores (z-score = (up-down) / $\sqrt{\text{count}}$, with up or down representing the number of up-regulated or down-regulated genes, respectively) that were used to determine whether the GO term maintained a higher proportion of up-regulated genes or down-regulated genes (D, E). The adjusted p-value came from the FDR value by PANTHER clustering (D, E). The size of the bubbles (D) represents the gene counts for each GO term.

Table 2
Differentially expressed transporters annotated by PANTHER GO-slim Molecular Function.

Category	Gene symbol	UniProt	Identified proteins of conserved domains	FDR	logFC
HMA2	PHYPADRAFT_125099	A9S7B1	Cadmium/zinc-transporting ATPase HMA2-related	1.13E−06	3.51
Phosphate transporter	PHYPADRAFT_65121	A9REM2	PitA (phosphate/sulfate permease); PHO4 (phosphate transporter family)	1.21E−11	−4.9
ABC	ppabcb6	A9TRT8	ATP-binding cassette transporter, subfamily B, member 6, group TAP protein	4.67E−04	6.92
	ppabcb8	A9TAL5	ATP-binding cassette transporter, subfamily B, member 8, group TAP protein	5.54E−05	6.79
	ppabcb16	A9TKP2	ATP-binding cassette transporter, subfamily B, member 16, group MDR/PGP protein	7.78E−05	−3.06
	ppabcb18	A9RU14	ATP-binding cassette transporter, subfamily B, member 18, group MDR/PGP protein	1.49E−07	6.83
	ppabcc15	A9U4I9	ATP-binding cassette transporter, subfamily C, member 15, group MRP protein	9.53E−05	8.07
	ppabcg23	A9TPG6	ATP-binding cassette transporter, subfamily G, member 23, group PDR protein	1.88E−10	8.38
XANP	PHYPADRAFT_181209	A9S4K1	Xanthine permease family; $HCO3^-$ transporter family	8.74E−13	8.42
V-ATPase	PHYPADRAFT_212771	A9SIT9	Vacuolar (H+)-ATPase V1, G subunit	6.38E−11	7.83
	PHYPADRAFT_139628	A9T345	Vacuolar (H+)-ATPase V1, C subunit	3.23E−21	−9.55
	PHYPADRAFT_106587	A9SJK8	Vacuolar (H+)-ATPase V1, B subunit	3.24E−05	2.42
PTR2	PHYPADRAFT_183911	A9SDW4	PTR2 (proton-dependent oligopeptide transporter family)	1.25E−05	6.79
	PHYPADRAFT_149487	A9TRK4	PTR2 (proton-dependent oligopeptide transporter family)	6.18E−05	3.91
SdaC	PHYPADRAFT_120356	A9RWA9	SdaC;SLC5-6-like_sbd (solute carrier families 5 and 6-like, solute binding domain)	1.83E−04	−2.81
	PHYPADRAFT_57709	A9SFZ0	SdaC;SLC5-6-like_sbd (solute carrier families 5 and 6-like, solute binding domain)	8.17E−07	6.74
Importin & exportin	PHYPADRAFT_193928[a]	A9TD66	Importin subunit beta 1	2.36E−08	7.19
	PHYPADRAFT_206059[a]	A9RVI5	Karyopherin importin beta 3	1.21E−11	−7.99
	PHYPADRAFT_217532[a]	A9SZV9	Importin-4	3.01E−27	−8.13
	PHYPADRAFT_168412[a]	A9T6U5	Im-13	1.71E−04	7.87
	PHYPADRAFT_193706[a]	A9TCE6	D-IMPORTIN 7/RANBP7	1.73E−08	−7.14
	PHYPADRAFT_218180[a]	A9T2C2	EXPORTIN 7	1.70E−04	8.27
Mitochondrial membrane transporter	PHYPADRAFT_172115	A9TV43	Mitochondrial inner membrane protein COX18; YidC (membrane protein insertase)	3.47E−08	7.56
	PHYPADRAFT_36810	A9TZR1	Tim23; Tim17/Tim22/Tim23/Pmp24 family	8.38E−06	−3.92
	PHYPADRAFT_171446	A9TQZ0	Mitochondrial carrier protein	2.45E−07	5.41
AKRs	PHYPADRAFT_213070[a]	A9SJP7	AKRs (aldo-keto reductases)	4.78E−09	7.47
	PHYPADRAFT_124662[a]	A9S6E7	AKRs (aldo-keto reductases)	6.53E−05	2.11
MFS	PHYPADRAFT_22469	A9RMV5	PLT5 (polyol transporter 5-related); MFS (major facilitator superfamily); sugar (and other) transporter	8.67E−08	2.88
	PHYPADRAFT_90589	A9TBH7	ZIF1 (protein zinc induced facilitator 1-related); MFS (major facilitator superfamily)	3.08E−04	7.22
	PHYPADRAFT_116273[a]	A9RKY4	MFS; sugar (and other) transporter	1.21E−04	6.66
Choline_transpo	PHYPADRAFT_119604	A9RUE8	Plasma-membrane choline transporter	2.58E−04	7.5
NaHE7	PHYPADRAFT_175277	A9RIV6	NhaP-type Na+/H+ or K+/H+ antiporter; cyclic nucleotide-binding domain	1.54E−04	−2.47
NaBC1	PHYPADRAFT_164885	A9SHF7	$HCO3^-$ transporter family	6.96E−20	9.39
CCC1_like	PHYPADRAFT_172945	A9U023	CCC1_like vacuolar iron/manganese importer	1.88E−08	−5.65
ATPase-Plipid	PHYPADRAFT_189702[a]	A9SY94	Phospholipid-translocating P-type ATPase, flippase	7.83E−04	−5.17
Arrestin_N	PHYPADRAFT_179943[a]	A9S037	Arrestin (or *S*-antigen), N-terminal domain	7.17E−06	6.76
ARM Repeat	PHYPADRAFT_91749[a]	A9TEL2	Arm repeat superfamily protein	5.20E−14	8.87
AMP-binding	PHYPADRAFT_181177[a]	A9S4H4	AMP-binding super family	3.34E−07	−6.60
SEC1A	SEC1A	A9U3H0	SM/Sec1-family protein	3.54E−04	7.33
VPS26	PHYPADRAFT_94096[a]	A9TKW8	Vps26 (vacuolar protein sorting-associated protein 26)	5.85E−04	7.93

[a] Genes identified as transporter activity but not transmembrane transporter activity in PANTHER GO-slim Molecular Function.

enriched vesicles by V-ATPases generated ΔpH (Salt and Wagner, 1993). A down-regulated gene was related to V-ATPase subunit C, which is a regulatory stator associating the peripheral V1 domain (site for ATP hydrolysis) and internal V0 domain (site for proton transport) together to control the assembly and the activity of V-ATPase (Jefferies et al., 2008; Smardon and Kane, 2007). Two up-regulated

Table 3
Differentially expressed genes that participate in vesicle-mediated transport by PANTHER GO-slim Biological Process annotation.

Category	Gene symbol	UniProt	Identified proteins of conserved domains	FDR	logFC
VPS26	PHYPADRAFT_94096	A9TKW8	Vps26 (vacuolar protein sorting-associated protein 26)	5.85E−04	7.93
Rab	RabD11	A9SLS3	Rab1/RabD-family small GTPase	1.69E−04	−3.40
	RabB11	A9TW31	Rab2/RabB-family small GTPase	2.23E−14	−8.49
	RabH22	A9U329	Rab6/RabH-family small GTPase	1.76E−07	−6.72
	RabG13	A9SB23	Rab7/RabG-family small GTPase	2.57E−04	8.08
REP1	PHYPADRAFT_139297	A9T2H0	Choroideremia RAB escort protein 1	1.72E−08	7.46
SNARE protein	VAMP72B2	A9TMZ3	VAMP72-family vesicle-associated membrane protein, R-SNARE	6.62E−07	7.62
	SEC22A2-2	A9SFZ8	SEC22-family vesicle-trafficking protein, R-SNARE	4.74E−07	6.76
	PHYPADRAFT_195156	A9THL0	SNARE motif, subgroup Qc	7.57E−06	7.18
SEC1A	SEC1A	A9U3H0	Sec1/Munc18-like (SM) proteins	3.54E−04	7.33
SEC8	PHYPADRAFT_112665	A9REH7	Sec8_exocyst superfamily; exocyst complex component 4	2.03E−05	8.80
SEC13	PHYPADRAFT_171600	A9TRZ5	Protein Sec13 homolog	4.55E−06	6.43
CHMP1B	PHYPADRAFT_207621	A9S101	Charged multivesicular body protein 1B	1.75E−04	7.70
Vesicle coat protein	PHYPADRAFT_158810	A9RFW2	Clathrin heavy chain	5.71E−17	−6.00
	PHYPADRAFT_216895	A9SXY8	Coatomer (COPI) alpha subunit C-terminus	2.72E−19	−9.24
	PHYPADRAFT_181209	A9RML7	Phosphatidylinositol-binding clathrin assembly protein LAP	2.29E−04	7.33
Act42A	PHYPADRAFT_226658	A9TYG3	Actin-42A-related; nucleotide-binding domain of the sugar kinase/HSP70/actin superfamily	7.86E−23	−9.81
TRAPPC8	PHYPADRAFT_147994	A9TN77	ER-Golgi trafficking TRAPP I complex 85 kDa subunit	2.91E−05	8.81
Cnx14D	PHYPADRAFT_59289	A9T349	Calnexin 14D-related	8.34E−04	−2.61
Golgin_A5	PHYPADRAFT_65712	A9RG82	Golgin subfamily A member 5 (Golgi structure maintaining protein)	4.35E−05	5.95
EG:86E4.5	PHYPADRAFT_33817	A9T6I5	Rho GAP superfamily	7.10E−04	6.93
	PHYPADRAFT_33820	A9U058	–	2.75E−04	7.23

Table 4
Differentially expressed genes relevant to antioxidant activities.

Category	Gene symbol	UniProt	Identified proteins of conserved domains	FDR	logFC
CAT	PHYPADRAFT_92315	A9TG35	Catalase	3.16E−19	−4.42
POD	PHYPADRAFT_56403	A9RXZ4	Peroxidase 28-related	1.88E−08	−5.05
GST	GSTF1	A9SCV0	Glutathione *S*-transferase 2	3.39E−17	−8.88
CCP	PHYPADRAFT_63071	Q8GU36	Ascorbate peroxidases and cytochrome *c* peroxidases	3.76E−05	−3.59
CYP13A2	PHYPADRAFT_119258	A9RU82	Cytochrome P450 CYP13A2-related	2.64E−05	2.60
SCO	PHYPADRAFT_134992	A9STB7	SCO (synthesis of cytochrome *c* oxidase) family	2.65E−05	7.32
PRX_1cys	PHYPADRAFT_161426	A9RWK3	Peroxiredoxin (PRX) family, 1-cys subfamily	3.52E−17	9.19
AKRs	PHYPADRAFT_213070	A9SJP7	AKRs (aldo-keto reductases)	4.78E−09	7.47
	PHYPADRAFT_124662	A9S6E7	AKRs (aldo-keto reductases)	6.53E−05	2.11
ARD	PHYPADRAFT_164159	A9SCJ6	1,2-Dihydroxy-3-keto-5-methylthiopentene dioxygenase 3	1.87E−04	7.93
MAPK3	PHYPADRAFT_167171	A9TD42	Mitogen-activated protein kinase 3	3.17E−07	3.32
	PHYPADRAFT_193902	A9SYS2	Mitogen-activated protein kinase 3	7.82E−06	6.49
MAPKKK	PHYPADRAFT_121101	A9RYD0	Mitogen-activated protein kinase kinase kinase YODA	6.08E−10	8.07
SAM1	PHYPADRAFT_60419	A9TJG9	*S*-adenosylmethionine synthase	1.40E−04	−4.16
DELLAb	DELLAb	A7U4T7	DELLA protein	9.06E−04	2.38
Hsp90	PHYPADRAFT_108065	A9TFM2	Heat shock protein Hsp 90-alpha-related	3.17E−10	−4.52
	PHYPADRAFT_221851	A9TFL9	Heat shock protein Hsp 90-alpha-related	8.25E−07	−6.46
	PHYPADRAFT_224556	A9TQU1	Heat shock protein Hsp 90-alpha-related	7.73E−06	−4.68
	PHYPADRAFT_216220	A9SVT7	Chaperone protein HTPG family protein-related; Hsp90 protein	5.55E−16	−8.71
Hsp70	PHYPADRAFT_58148	A9SLL3	Heat shock-related 70 kDa protein 2	4.40E−09	−7.30
	PHYPADRAFT_96217	A9TRK2	Heat shock-related 70 kDa protein 2	3.60E−06	−6.15
GLP3b	PpGLP3b	A9SDF7	Germin-like protein subfamily 3 member 1-related	1.94E−07	−3.06
GLP4	PHYPADRAFT_151453	A9TVN1	Germin-like protein subfamily 2 member 1-related	1.90E−07	−2.59

genes were related respectively to subunit B, which forms ATP binding sites along with subunit A, and subunit G, which form crosslinks along subunit B and interact with subunit C (Jefferies et al., 2008).

For the peptide transporter (PTR) family on the vacuole membrane, some members have roles for plant defenses under biotic and abiotic stress (Dietrich et al., 2004; Karim et al., 2007), while others may serve as secondary metabolite transporters (Nour-Eldin et al., 2012). The up-regulated PTR2 has been discovered as a tonoplast-localized H^+ cotransporter, which recognizes dipeptides and tripeptides with high affinity (Chiang et al., 2004; Nour-Eldin and Halkier, 2013), indicating promotion of vacuole export in *M. fortunei*.

4.3. Vesicle trafficking and fusion

Twenty-four genes were annotated to have functions in vesicle-mediated transport by the PantherGO-slim Biological Process category, from which 22 genes with specific proteins are presented in Table 3, with Vps26 and SEC1 also playing roles in the transporter activity (Table 2).

The up-regulated VPS26 (vacuolar protein sorting-associated proteins, VPS), as a subunit of the retromer complex, may confer cadmium detoxification by vacuolar degradation in yeast (Guo et al., 2016). VPS26 shares a close architecture with arrestins (Shi et al., 2006), a trafficking adaptor family regulating endocytosis by connecting G-protein coupled receptors (GPCRs) to clathrin (Gurevich and Gurevich, 2006), which were also up-regulated in *M. fortunei* (Table 2).

The results might correlate with the "vesicle fusion" category by the *Physcomitrella patens* annotation in DAVID (Fig. 4A), with 3 up-regulated genes functioning as relevant to SNARE binding, SNARE complex, SNAP receptor activity and vesicle fusion simultaneously. Soluble *N*-ethylmaleimide-sensitive factor attachment protein receptors (SNARE) have roles in vesicle trafficking and membrane fusion and are classified as t-SNAREs (that are targeted at a membrane, and can be further classified as Qa-, Qb-, and Qc-SNAREs) and v-SNAREs (that are targeted at a vesicle, and are also known as R-SNAREs) (Crawford and Kavalali, 2015; L. Zhang et al., 2017). Three genes were functioned as relevant to "vesicle fusion" by DAVID, and all were up-regulated in *M. fortunei* roots. In addition to the one up-regulated SNARE_Qc gene, the others were identified as the SEC22-family (SEC22A2, involved in ER-to-Golgi vesicle trafficking) and VAMP72-family (VAMP72B2, involved in secretion, vesicle trafficking to the plasma membrane) of the v-SNARE proteins. As VAMP72-family members, R-SNAREs VAMP721 and VAMP722 can bind with t-SNARE SYP121 (B. Zhang et al., 2017) to drive membrane fusion, while SYP121 can fuse with a heavy metal transporter, MerC, to target and express at the plasma membrane, which further increases cadmium accumulation and tolerance, consequently, in *Arabidopsis thaliana* (Kiyono et al., 2012).

Other membrane trafficking regulatory proteins, such as SEC1A, SEC8, and SEC13, were also up-regulated in cadmium-treated *M. fortunei* roots. The SEC1 proteins in the Sec1/Munc18-like (SM) family are known for spatially and temporally organizing t-SNAREs, which further leads to the fusogenic action of t-SNAREs with v-SNAREs at the membrane (Südhof and Rothman, 2009). SEC8, as one of the eight subunits of the exocyst complex, serves for the docking between post-Golgi vesicles and the plasma membrane (Kulich et al., 2015).

As SNARE facilitates the vesicle-membrane fusion process, Rab GTPases serve to regulate the formation, uncoating, and transport of vesicles (Hutagalung and Novick, 2011; Paul et al., 2014). The down-regulated Rab genes in subfamilies RabD, RabB and RabH regulate the ER-Golgi traffic, Golgi&ERGIC-ER retrograde traffic, and intra-Golgi traffic, respectively, while the up-regulated RabG subfamily controls the late endocytic pathway, with vesicle transport to the lysosome, laterendosome or other recycling compartments (Fang and Chao, 2014; Hutagalung and Novick, 2011). RabG genes, with a 'response to stimulus' function in biological processes, have been identified to be involved in the tolerance to salt, osmotic stress, mannitol and abscisic acid (ABA) in plants (Pitakrattananukool et al., 2012). Membrane-associated Rabs, such as Rab1 (Chen and Balch, 2006) and Rab3 (Sakisaka et al., 2002), are recycled by the functional GDI (guanine nucleotide dissociation inhibitor)-Hsp90 (heat shock protein 90) complex, while Hsp90 (Table 4) was also down-regulated in the *M. fortunei* roots.

Thus, the differentially expressed arrestins and VPS, SNARE, SEC and Rab proteins in *M. fortunei* might indicate an increasing expression of heavy metal transporters mediated by cell signaling, vesicle trafficking and the fusion process.

4.4. Antioxidant system

Cadmium, as a non-redox-reactive heavy metal, could indirectly induce oxidative stress by blocking functional biomolecules, causing reactive oxygen species (ROS) accumulation, which further leads to protein oxidation, membrane lipid peroxidation and even DNA injury (Éva et al., 2014; Schutzendubel and Polle, 2002). To cope with the Cd-induced

Table 5
Differentially expressed genes relevant to energy release and primary metabolic processes.

Functional category	Name	Gene Symbol	UniProt	Identified proteins of conserved domains	FDR	logFC
TCA cycle; glycolysis; pentose phosphate pathway; ascorbate and aldarate metabolism	DLD	PHYPADRAFT_106783	A9SNH9	Dihydrolipoyl dehydrogenase, mitochondrial	1.35E−05	−5.96
	ENO2	PHYPADRAFT_63926	A9RBJ9	Bifunctional enolase 2/Transcriptional activator	1.13E−05	−3.29
	GME	PHYPADRAFT_168267	A9T619	GDP-D-mannose-3′,5′-epimerase	1.38E−06	−6.31
	ALDH7A	ALDH7A	A9TIC4	Alpha-aminoadipic semialdehyde dehydrogenase	8.82E−05	5.58
	G6PDH	PHYPADRAFT_110351	A9TFZ3	Glucose-6-phosphate 1-dehydrogenase	1.65E−06	6.60
	GDPGP1	PHYPADRAFT_166416	A9SSY3	GDP-D-glucose phosphorylase 1	2.88E−17	9.05
Glycine, serine and threonine metabolism; glyoxylate and dicarboxylate metabolism	SHMT	PHYPADRAFT_129878	A9SHC0	Serine hydroxymethyltransferase, cytosolic	1.82E−07	−6.72
	GLDC	PHYPADRAFT_171132	A9TNZ8	Glycine dehydrogenase decarboxylating, mitochondrial	4.01E−20	−6.34
	HAO1	PHYPADRAFT_161490	A9RWX7	Hydroxy acid oxidase 1	1.54E−05	−5.96
	CAT[a]	PHYPADRAFT_92315	A9TG35	Catalase	3.16E−19	−4.42
Pantothenate and CoA biosynthesis	DPD	PHYPADRAFT_73095	A9S0U7	Dihydropyrimidine dehydrogenase [NADP+]	1.77E−05	2.38
Fatty acid elongation; fatty acid degradation	KCS-11	PHYPADRAFT_195698	A9TJJ8	3-Ketoacyl-CoA synthase 11	4.86E−14	4.04
	PSE1	PHYPADRAFT_95302	Q8S4Q5	Polyunsaturated fatty acid specific elongation enzyme 1	5.52E−06	6.45
	acyl-CoA oxidase	PHYPADRAFT_207164	A9RZ70	Acyl-coenzyme A oxidase	1.03E−05	6.19
	CDKA2	CDKA;2	A9TPJ3	Cyclin-dependent kinase 2	8.40E−07	−6.46
	Bet_v1_like	PHYPADRAFT_72516	A9RZA3	Ligand-binding bet_v_1 domain of major pollen allergen of *Betula verrucosa*	7.37E−10	−7.53
Valine, leucine and isoleucine degradation	NAD_binding_11	PHYPADRAFT_205200	A9RSI5	3-Hydroxyisobutyrate dehydrogenase, mitochondrial	9.47E−04	5.33
Purine metabolism; nicotinate and nicotinamide metabolism	SurE	PHYPADRAFT_46129	A9SJL1	Survival protein SurE	2.52E−04	−5.17
	GLP4[a]	PHYPADRAFT_151453	A9TVN1	Germin-like protein subfamily 2 member 1-related	1.90E−07	−2.59
	AKRs[a]	PHYPADRAFT_124662	A9S6E7	AKRs (aldo-keto reductases); Tas (predicted oxidoreductase, related to aryl-alcohol dehydrogenase)	6.53E−05	2.11
Riboflavin metabolism	RibC	PHYPADRAFT_125797	A9S8S3	Riboflavin kinase	8.35E−07	−6.46
Porphyrin and chlorophyll metabolism	PBG-deaminase	PHYPADRAFT_197854	A9TSP6	Porphobilinogen deaminase	7.83E−04	−5.17
Cysteine and methionine metabolism; arginine biosynthesis; phenylalanine metabolism; phenylalanine, tyrosine and tryptophan biosynthesis; phenylpropanoid biosynthesis	SAM1[a]	PHYPADRAFT_60419	A9TJG9	*S*-adenosylmethionine synthase	1.40E−04	−4.16
	M20_ArgE-related	PHYPADRAFT_175929	A9RKM4	M20 peptidases with similarity to acetylornithine deacetylases	6.11E−07	−6.15
	PER28[a]	PHYPADRAFT_56403	A9RXZ4	Peroxidase 28-related	1.88E−08	−5.05
	PLN02397	PHYPADRAFT_102134	A9U4V4	Aspartate aminotransferase, cytoplasmic	1.84E−04	7.17
	PAL3	PHYPADRAFT_121522	A9RYH4	Phenylalanine ammonia-lyase 3	1.35E−05	6.22
	PRX_1cys[a]	PHYPADRAFT_161426	A9RWK3	Peroxiredoxin (PRX) family, 1-cys subfamily	3.52E−17	9.19
	MAPKKK[a]	PHYPADRAFT_121101	A9RYD0	Mitogen-activated protein kinase kinase kinase YODA	6.08E−10	8.07
Brassinosteroid biosynthesis	CYP13A2[a]	PHYPADRAFT_119258	A9RU82	Cytochrome P450 CYP13A2-related	2.64E−05	2.60
Ubiquinone and other terpenoid-quinone biosynthesis	SpoVK	PHYPADRAFT_203033	A9RJL4	Fidgetin-like protein 1	7.83E−04	−5.17
Steroid biosynthesis	5-DES	PHYPADRAFT_135889	A9SV27	Fatty acid hydroxylase superfamily, C-5 sterol desaturase	7.23E−04	−3.09

[a] Genes also identified relevant to antioxidant activities in Table 4.

oxidative stresses, small molecule metabolites such as ABA (ascorbic acid) and GSH (reduced glutathione), and antioxidative enzymes such as CAT (catalase) and POD (peroxidase) compose the plant ROS-scavenging system (Tkalec et al., 2008), and 23 relevant genes were selected for better presentation of the antioxidant mechanism in the *M. fortunei* roots. The increase in antioxidant levels were also identified as a major cadmium detoxifying mechanism in the roots of *Microsorum pteropus* (Lan et al., 2018a; Lan et al., 2018b), which is a Cd hyperaccumulator as well as a close relative to *M. fortunei*.

On one hand, the down-regulation of CAT (catalase), POD (peroxidase 28), GST (glutathione *S*-transferase), CCP (cytochrome *c* peroxidase), and the up-regulation of MAPK (mitogen-activated protein kinase) indicated cadmium-induced oxidative damage under ROS accumulation in *M. fortunei* roots. The depletion of ROS-scavenging CAT and GSH is a critical symptom of cadmium toxicity (Schutzendubel and Polle, 2002). The GST could reduce Cd toxicity and root-shoot translocation by catalyzing Cd complexation with GSH and scavenging H_2O_2 with the expense of GSH (Radadiya et al., 2016; Zhang et al., 2013). The MAPK3 (Liu et al., 2010) was found to be activated by cadmium, relying on a signal transduction pathway regulated by the ROS accumulation levels. The ROS scavenger GSH was found to significantly decrease the Cd-induced MAPK3 activation in Arabidopsis. These symptoms revealed that *M. fortunei* roots were physiologically impaired under 1000-μmol/L Cd exposure.

On the other hand, the up-regulation of cytochrome P450, 1-cys peroxiredoxin (PRX) and AKRs (aldo-keto reductases) indicated a potential antioxidant mechanism under Cd stress. Cytochrome P450 enzymes are known for their role in plant defenses by the oxidative degradation of environmental toxins (Werck-Reichhart and Feyereisen, 2000). The 1-Cys PRX family proteins were found to protect against cadmium-induced oxidative stress in yeast mitochondria (Greetham and Grant, 2009), with GSH being the physiological electron donor.

Moreover, cadmium-induced ROS could interact with membrane(s), causing lipid peroxidation and producing lipid peroxide breakdown products such as malondialdehyde (MDA), which lead to oxidative cellular damage (Éva et al., 2014). Stress-induced AKR enzymes could eliminate reactive aldehydes produced by lipid peroxidation (Éva et al., 2014), and their genes were also up-regulated in *M. fortunei* roots.

Apart from the antioxidative enzymes, other defense responses, such as the underexpression of SAM1 and overexpression of DELLAs, could help to reduce ROS accumulation in *M. fortunei* roots, while plant hormones, such as abscisic acid (ABA), gibberellin (GA) and ethylene, might play important roles in these detoxification mechanisms. SAMS (*S*-adenosylmethionine synthase) catalyzes the synthesis of SAM (*S*-adenosylmethionine), which is a precursor of the polyamine and ethylene biosynthesis pathway (Radadiya et al., 2016). SAM1 in *Medicago sativa* subsp. *falcata* could be mediated by ABA, H_2O_2 and NO interactions, and its accumulations were found to promote polyamine synthesis and oxidation by amine oxidases, which further generate H_2O_2 (Guo et al., 2014; Radadiya et al., 2016). Up-regulated DELLAs, as transcriptional repressors in the GA signaling pathway (Dobrikova et al., 2017), were found to restrain ROS accumulation in *Arabidopsis thaliana* (Colebrook et al., 2014), with the accumulation of DELLAs mediated by ABA under a limited bioactive GA level. Both down-regulated HSP70s (Heat Shock-Related 70 kDa proteins) (Li et al., 2014; Tkalec et al., 2008) and GLPs (germin-like proteins) (Li et al., 2010) were found to be controlled by an ABA-dependent H_2O_2-related signaling pathway under cadmium stress, while no specific mechanism has been identified. Meanwhile, ABA, ethylene and GA signaling pathways were discovered to be closely integrated (Colebrook et al., 2014), indicating the potential critical role of phytohormones as a Cd-tolerant mechanism in *M. fortunei*.

4.5. Energy release and primary metabolic processes

In addition to phytohormones as primary metabolites, other genes related to energy release and primary metabolic processes (such as citrate cycle (TCA cycle), glycolysis/gluconeogenesis, pentose phosphate pathway, ascorbate and aldarate metabolism, glycine, serine and threonine metabolism, α-linolenic acid metabolism, fatty acid elongation and degradation, and steroid, ubiquinone and other terpenoid-quinone biosynthesis) might play a role in response to cadmium exposure (Table 5).

For the 27 relevant genes, some might be differentially expressed as a consequence of Cd toxification, such as the down-regulated dihydrolipoamide dehydrogenase (DLD), which mediates Actyl-CoA formation in the TCA cycle, catalyzes the formation of lipid-soluble antioxidant ubiquinol by reducing ubiquinone and is Cd-enhanced in *Arabidopsis* (Cai et al., 2011). Some of the genes might participate in detoxification mechanisms, such as the up-regulated ALDH7A that could play a similar detoxifying role with AKRs by removing lipid-peroxidation-induced aldehydes (Brocker et al., 2010), while the overexpressed G6PDH could help to maintain the NADPH level to further maintain the GSH level (Thomas et al., 1991).

5. Conclusion

In conclusion, *M. fortunei* may serve as a potential cadmium-hypertolerant plant in which most cadmium is sequestered and detoxified in the roots, with minimized root-to-shoot translocation to guarantee the photosynthetic capacity in the more Cd-sensitive leaves. *M. fortunei* could accumulate >2000 μg/g DW Cd under 1000 μmol/L Cd exposure, with few symptoms of Cd-induced phytotoxicity effects. Cadmium could be accumulated and sequestered in *M. fortunei* roots by transporters such as ABCs and V-ATPases, with genes encoding vesicle trafficking and fusion mediating the heavy metal transporter-targeting or ligand-chelating processes. Further, the cadmium defense mechanism might be a function of antioxidative enzymes, non-enzymatic antioxidants, plant hormones and other primary metabolites.

Supplementary data to this article can be found online at https://doi.org/10.1016/j.scitotenv.2018.08.281.

Acknowledgments

This study was funded by the National Science Foundation of China (NSFC) (31570508). This work is also supported by the Undergraduate Student Research Training Program of the Ministry of Education of the People's Republic of China, the High-performance Computing Platform of Peking University in China and the Tsinghua National Laboratory for Information Science and Technology in China.

References

Arnot, J.A., Gobas, F.A., 2006. A review of bioconcentration factor (BCF) and bioaccumulation factor (BAF) assessments for organic chemicals in aquatic organisms. Environ. Rev. 14, 257–297. https://doi.org/10.1139/a06-005.

Baker, A.J., Brooks, R., Pease, A., Malaisse, F., 1983. Studies on copper and cobalt tolerance in three closely related taxa within the genus *Silene* L. (Caryophyllaceae) from Zaïre. Plant Soil 73, 377–385. https://doi.org/10.1007/BF02184314.

Basa, B., Lattanzio, G., Solti, Á., Tóth, B., Abadía, J., Fodor, F., Sárvári, É., 2014. Changes induced by cadmium stress and iron deficiency in the composition and organization of thylakoid complexes in sugar beet (*Beta vulgaris* L.). Environ. Exp. Bot. 101, 1–11. https://doi.org/10.1016/j.envexpbot.2013.12.026.

Beard, S.J., Hashim, R., Wu, G.-H., Binet, M.R., Hughes, M.N., Poole, R.K., 2000. Evidence for the transport of zinc (II) ions via the pit inorganic phosphate transport system in *Escherichia coli*. FEMS Microbiol. Lett. 184, 231–235. https://doi.org/10.1111/j.1574-6968.2000.tb09019.x.

Brocker, C., Lassen, N., Estey, T., Pappa, A., Cantore, M., Orlova, V.V., Chavakis, T., Kavanagh, K.L., Oppermann, U., Vasiliou, V., 2010. Aldehyde dehydrogenase 7A1 (ALDH7A1) is a novel enzyme involved in cellular defense against hyperosmotic stress. J. Biol. Chem. 285, 18452–18463. https://doi.org/10.1074/jbc.M109.077925.

Buchfink, B., Xie, C., Huson, D.H., 2015. Fast and sensitive protein alignment using DIAMOND. Nat. Methods 12, 59. https://doi.org/10.1038/nmeth.3176.

Cai, Y., Cao, F.-B., Wei, K., Zhang, G.-P., Wu, F.-B., 2011. Genotypic dependent effect of exogenous glutathione on Cd-induced changes in proteins, ultrastructure and antioxidant defense enzymes in rice seedlings. J. Hazard. Mater. 192, 1056–1066. https://doi.org/10.1016/j.jhazmat.2011.06.011.

Çakır, B., Kılıçkaya, O., 2013. Whole-genome survey of the putative ATP-binding cassette transporter family genes in *Vitis vinifera*. PLoS One 8, e78860. https://doi.org/10.1371/journal.pone.0078860.

Chen, C.Y., Balch, W.E., 2006. The Hsp90 chaperone complex regulates GDI-dependent Rab recycling. Mol. Biol. Cell 17, 3494–3507. https://doi.org/10.1091/mbc.e05-12-1096.

Chen J, Gilbert M (2006) Flora of China. Science, Beijing and Missouri Botanical Garden Press, St Louis.

Chen, Y.-S., Lun, A.T., Smyth, G.K., 2014. Differential expression analysis of complex RNA-seq experiments using edgeR. In: Datta, S.N.D. (Ed.), Statistical Analysis of Next Generation Sequencing Data. Springer, Cham, pp. 51–74 https://doi.org/10.1007/978-3-319-07212-8_3.

Chiang, C.-S., Stacey, G., Tsay, Y.-F., 2004. Mechanisms and functional properties of two peptide transporters, AtPTR2 and fPTR2. J. Biol. Chem. 279, 30150–30157. https://doi.org/10.1074/jbc.M405192200.

Clemens, S., 2006. Toxic metal accumulation, responses to exposure and mechanisms of tolerance in plants. Biochimie 88, 1707–1719. https://doi.org/10.1016/j.biochi.2006.07.003.

Colebrook, E.H., Thomas, S.G., Phillips, A.L., Hedden, P., 2014. The role of gibberellin signalling in plant responses to abiotic stress. J. Exp. Biol. 217, 67–75. https://doi.org/10.1242/jeb.089938.

Crawford, D.C., Kavalali, E.T., 2015. Molecular underpinnings of synaptic vesicle pool heterogeneity. Traffic 16, 338–364. https://doi.org/10.1111/tra.12262.

Dietrich, D., Hammes, U., Thor, K., Suter-Grotemeyer, M., Flückiger, R., Slusarenko, A.J., Ward, J.M., Rentsch, D., 2004. AtPTR1, a plasma membrane peptide transporter expressed during seed germination and in vascular tissue of *Arabidopsis*. Plant J. 40, 488–499. https://doi.org/10.1111/j.1365-313X.2004.02224.x.

Dobrikova, A.G., Yotsova, E.K., Börner, A., Landjeva, S.P., Apostolova, E.L., 2017. The wheat mutant DELLA-encoding gene (Rht-B1c) affects plant photosynthetic responses to cadmium stress. Plant Physiol. Biochem. 114, 10–18. https://doi.org/10.1016/j.plaphy.2017.02.015.

Eastmond, P.J., Quettier, A.-L., Kroon, J.T., Craddock, C., Adams, N., Slabas, A.R., 2010. Phosphatidic acid phosphohydrolase1 and 2 regulate phospholipid synthesis at the endoplasmic reticulum in *Arabidopsis*. Plant Cell 22, 2796–2811. https://doi.org/10.1105/tpc.109.071423.

Éva, C., Tóth, G., Oszvald, M., Tamás, L., 2014. Overproduction of an *Arabidopsis* aldo–keto reductase increases barley tolerance to oxidative and cadmium stress by an in vivo reactive aldehyde detoxification. Plant Growth Regul. 74, 55–63. https://doi.org/10.1007/s10725-014-9896-x.

Fang, W., Chao, L., 2014. The classification and function of plant Rab GTPases. Chin. J. Biochem. Mol. Biol. 8, 005 (in Chinese).

Feng, J.-J., Jia, W.-T., Lv, S.-L., Bao, H.-X., Ge, D.-L., Miao, F.-F., Zhang, X., Wang, J.-H., Li, J.-H., Li, D.-S., Zhu, C., 2018. Comparative transcriptome combined with morpho-physiological analyses revealed key factors for differential cadmium accumulation in two contrasting sweet sorghum genotypes. Plant Biotechnol. J. 16, 558–571. https://doi.org/10.1111/pbi.12795.

Fu, L.-M., Niu, B.-F., Zhu, Z.-W., Wu, S.-T., Li, W.-Z., 2012. CD-HIT: accelerated for clustering the next-generation sequencing data. Bioinformatics 28, 3150–3152. https://doi.org/10.1093/bioinformatics/bts565.

Gallego, S.M., Pena, L.B., Barcia, R.A., Azpilicueta, C.E., Iannone, M.F., Rosales, E.P., Zawoznik, M.S., Groppa, M.D., Benavides, M.P., 2012. Unravelling cadmium toxicity and tolerance in plants: insight into regulatory mechanisms. Environ. Exp. Bot. 83, 33–46. https://doi.org/10.1016/j.envexpbot.2012.04.006.

Geisler, M., 2014. Plant ABC Transporters. Springer International Publishing, Switzerland https://doi.org/10.1007/978-3-319-06511-3.

Grabherr, M.G., Haas, B.J., Yassour, M., Levin, J.Z., Thompson, D.A., Amit, I., Adiconis, X., Fan, L., Raychowdhury, R., Zeng, Q.-D., 2011. Full-length transcriptome assembly from RNA-Seq data without a reference genome. Nat. Biotechnol. 29, 644. https://doi.org/10.1038/nbt.1883.

Greetham, D., Grant, C.M., 2009. Antioxidant activity of the yeast mitochondrial one-Cys peroxiredoxin is dependent on thioredoxin reductase and glutathione in vivo. Mol. Cell. Biol. 29, 3229–3240. https://doi.org/10.1128/MCB.01918-08.

Guo, Z.-F., Tan, J.-L., Zhuo, C.-L., Wang, C.-Y., Xiang, B., Wang, Z.-Y., 2014. Abscisic acid, H2O2 and nitric oxide interactions mediated cold-induced S-adenosylmethionine synthetase in *Medicago sativa* subsp. falcata that confers cold tolerance through up-regulating polyamine oxidation. Plant Biotechnol. J. 12, 601–612. https://doi.org/10.1111/pbi.12166.

Guo, L., Ganguly, A., Sun, L.-L., Suo, F., Du, L.-L., Russell, P., 2016. Global fitness profiling identifies arsenic and cadmium tolerance mechanisms in fission yeast. G3 Genes Genomes Genet. 6, 3317–3333. https://doi.org/10.1534/g3.116.033829.

Gurevich, V.V., Gurevich, E.V., 2006. The structural basis of arrestin-mediated regulation of G-protein-coupled receptors. Pharmacol. Ther. 110, 465–502. https://doi.org/10.1016/j.pharmthera.2005.09.008.

Huang, D.-W., Sherman, B.T., Lempicki, R.A., 2008. Systematic and integrative analysis of large gene lists using DAVID bioinformatics resources. Nat. Protoc. 4, 44. https://doi.org/10.1038/nprot.2008.211.

Hutagalung, A.H., Novick, P.J., 2011. Role of Rab GTPases in membrane traffic and cell physiology. Physiol. Rev. 91, 119–149. https://doi.org/10.1152/physrev.00059.2009.

IARC, 1993. International Agency for Research on Cancer-summaries & evaluations: cadmium and cadmium compounds (Group 1). IARChttp://www.inchem.org/documents/iarc/vol58/mono58-2.html, Accessed date: 1 June 2017.

ITRC, 2010. Phytotechnologies. Interstate Technology & Regulatory Council, Mining Waste Team, Washington, D.C. www.itrcweb.org, Accessed date: 1 June 2017.

Jackson, R.J., Binet, M.R., Lee, L.J., Ma, R., Graham, A.I., McLeod, C.W., Poole, R.K., 2008. Expression of the PitA phosphate/metal transporter of *Escherichia coli* is responsive to zinc and inorganic phosphate levels. FEMS Microbiol. Lett. 289, 219–224. https://doi.org/10.1111/j.1574-6968.2008.01386.x.

Jefferies, K.C., Cipriano, D.J., Forgac, M., 2008. Function, structure and regulation of the vacuolar (H+)-ATPases. Arch. Biochem. Biophys. 476, 33–42. https://doi.org/10.1016/j.abb.2008.03.025.

Kalaji, M.H., Goltsev, V.N., Żuk-Gołaszewska, K., Zivcak, M., Brestic, M., 2017. Chlorophyll Fluorescence: Understanding Crop Performance—Basics and Applications. CRC Press.

Karim, S., Holmström, K.-O., Mandal, A., Dahl, P., Hohmann, S., Brader, G., Palva, E.T., Pirhonen, M., 2007. AtPTR3, a wound-induced peptide transporter needed for defence against virulent bacterial pathogens in *Arabidopsis*. Planta 225, 1431–1445. https://doi.org/10.1007/s00425-006-0451-5.

Kiyono, M., Oka, Y., Sone, Y., Tanaka, M., Nakamura, R., Sato, M.H., Pan-Hou, H., Sakabe, K., Inoue, K.-i., 2012. Expression of the bacterial heavy metal transporter MerC fused with a plant SNARE, SYP121, in *Arabidopsis thaliana* increases cadmium accumulation and tolerance. Planta 235, 841–850. https://doi.org/10.1007/s00425-011-1543-4.

Klughammer, C., Schreiber, U., 2008. Complementary PS II quantum yields calculated from simple fluorescence parameters measured by PAM fluorometry and the Saturation Pulse method. PAM Appl. Notes 1, 201–247.

Kučera, T., Horáková, H., Šonská, A., 2008. Toxic metal ions in photoautotrophic organisms. Photosynthetica 46, 481–489. https://doi.org/10.1007/s11099-008-0083-z.

Kulich, I., Vojtíková, Z., Glanc, M., Ortmannová, J., Rasmann, S., Žárský, V., 2015. Cell wall maturation of *Arabidopsis* trichomes is dependent on exocyst subunit EXO70H4 and involves callose deposition. Plant Physiol. 168, 120–131. https://doi.org/10.1104/pp.15.00112.

Küpper, H., Zhao, F.-J., McGrath, S.P., 1999. Cellular compartmentation of zinc in leaves of the hyperaccumulator *Thlaspi caerulescens*. Plant Physiol. 119, 305–312. https://doi.org/10.1104/pp.119.1.305.

Küpper, H., Lombi, E., Zhao, F.-J., McGrath, S.P., 2000. Cellular compartmentation of cadmium and zinc in relation to other elements in the hyperaccumulator *Arabidopsis halleri*. Planta 212, 75–84. https://doi.org/10.1007/s004250000366.

Lan, X.-Y., Wang, J.-J., Yan, Y.-Y., Li, X.-Y., Xu, F.-L., 2017. Hyperaccumulation capacity and resistance physiology of *Microsorum pteropus*, an aquatic fern to cadmium. Sci. Sin. Vitae 47, 1113–1123 (in Chinese).

Lan, X.-Y., Yan, Y.-Y., Yang, B., Li, X.-Y., Xu, F.-L., 2018a. Differential expression of proteins in the leaves and roots of cadmium-stressed *Microsorum pteropus*, a novel potential aquatic cadmium hyperaccumulator. Sci. Total Environ. 642, 1369–1377. https://doi.org/10.1016/j.scitotenv.2018.06.168.

Lan, X.-Y., Yang, B., Yan, Y.-Y., Li, X.-Y., Xu, F.-L., 2018b. Resistance mechanisms and their difference between the root and leaf of *Microsorum pteropus*–a novel potential aquatic cadmium hyperaccumulator. Sci. Total Environ. 616, 480–490. https://doi.org/10.1016/j.scitotenv.2017.10.271.

Langmead, B., Trapnell, C., Pop, M., Salzberg, S.L., 2009. Ultrafast and memory-efficient alignment of short DNA sequences to the human genome. Genome Biol. 10, R25. https://doi.org/10.1186/gb-2009-10-3-r25.

Li, B., Dewey, C.N., 2011. RSEM: accurate transcript quantification from RNA-Seq data with or without a reference genome. BMC Bioinforma. 12, 323. https://doi.org/10.1186/1471-2105-12-323.

Li, W.-Z., Godzik, A., 2006. Cd-hit: a fast program for clustering and comparing large sets of protein or nucleotide sequences. Bioinformatics 22, 1658–1659. https://doi.org/10.1093/bioinformatics/btl158.

Li, H., Handsaker, B., Wysoker, A., Fennell, T., Ruan, J., Homer, N., Marth, G., Abecasis, G., Durbin, R., 2009. The sequence alignment/map format and SAMtools. Bioinformatics 25, 2078–2079. https://doi.org/10.1093/bioinformatics/btp352.

Li, H.-Y., Jiang, J., Wang, S., Liu, F.-F., 2010. Expression analysis of ThGLP, a new germin-like protein gene, in *Tamarix hispida*. J. For. Res. 21, 323–330. https://doi.org/10.1007/s11676-010-0078-z.

Li, P.-Y., Huo, L.-N., Su, W., Lu, R.-M., Deng, C.-C., Lv, Y.-G., 2011. Detection of antioxidative capacity of *Microsorum fortunei* extract by ABTS assay. Chin. J. Exp. Tradit. Med. Formulae 1, 049 (in Chinese).

Li, H., Liu, S.S., Yi, C.Y., Wang, F., Zhou, J., Xia, X.J., Shi, K., Zhou, Y.H., Yu, J.Q., 2014. Hydrogen peroxide mediates abscisic acid-induced HSP70 accumulation and heat tolerance in grafted cucumber plants. Plant Cell Environ. 37, 2768–2780. https://doi.org/10.1111/pce.12360.

Liu, X.-M., Kim, K.E., Kim, K.-C., Nguyen, X.C., Han, H.J., Jung, M.S., Kim, H.S., Kim, S.H., Park, H.C., Yun, D.-J., 2010. Cadmium activates *Arabidopsis* MPK3 and MPK6 via accumulation of reactive oxygen species. Phytochemistry 71, 614–618. https://doi.org/10.1016/j.phytochem.2010.01.005.

McCarthy, S., Ai, C., Wheaton, G., Tevatia, R., Eckrich, V., Kelly, R., Blum, P., 2014. Role of an archaeal PitA transporter in the copper and arsenic resistance of *Metallosphaera sedula*, an extreme thermoacidophile. J. Bacteriol. 196, 3562–3570. https://doi.org/10.1128/JB.01707-14.

Mendoza-Cózatl, D.G., Jobe TO, Hauser, F., Schroeder, J.I., 2011. Long-distance transport, vacuolar sequestration, tolerance, and transcriptional responses induced by cadmium and arsenic. Curr. Opin. Plant Biol. 14, 554–562. https://doi.org/10.1016/j.pbi.2011.07.004.

Mi, H.-Y., Dong, Q., Muruganujan, A., Gaudet, P., Lewis, S., Thomas, P.D., 2009. PANTHER version 7: improved phylogenetic trees, orthologs and collaboration with the Gene Ontology Consortium. Nucleic Acids Res. 38, D204–D210. https://doi.org/10.1093/nar/gkp1019.

Mietkiewska, E., Siloto, R.M., Dewald, J., Shah, S., Brindley, D.N., Weselake, R.J., 2011. Lipins from plants are phosphatidate phosphatases that restore lipid synthesis in a pah1Δ mutant strain of *Saccharomyces cerevisiae*. FEBS J. 278, 764–775. https://doi.org/10.1111/j.1742-4658.2010.07995.x.

Murphy, A.S., Peer, W., Schulz, B., 2010. The Plant Plasma Membrane. vol. 19. Springer Science & Business Media. https://doi.org/10.1007/978-3-642-13431-9.

Nakamura, Y., Koizumi, R., Shui, G.-H., Shimojima, M., Wenk, M.R., Ito, T., Ohta, H., 2009. *Arabidopsis* lipins mediate eukaryotic pathway of lipid metabolism and cope critically with phosphate starvation. Proc. Natl. Acad. Sci. 106, 20978–20983. https://doi.org/10.1073/pnas.0907173106.

Nour-Eldin, H.H., Halkier, B.A., 2013. The emerging field of transport engineering of plant specialized metabolites. Curr. Opin. Biotechnol. 24, 263–270. https://doi.org/10.1016/j.copbio.2012.09.006.

Nour-Eldin, H.H., Andersen, T.G., Burow, M., Madsen, S.R., Jørgensen, M.E., Olsen, C.E., Dreyer, I., Hedrich, R., Geiger, D., Halkier, B.A., 2012. NRT/PTR transporters are essential for translocation of glucosinolate defence compounds to seeds. Nature 488, 531. https://doi.org/10.1038/nature11285.

Paul, P., Simm, S., Mirus, O., Scharf, K.-D., Fragkostefanakis, S., Schleiff, E., 2014. The complexity of vesicle transport factors in plants examined by orthology search. PLoS One 9, e97745. https://doi.org/10.1371/journal.pone.0097745.

Pitakrattananukool, S., Kawakatsu, T., Anuntalabhochai, S., Takaiwa, F., 2012. Overexpression of OsRab7B3, a small GTP-binding protein gene, enhances leaf senescence in transgenic rice. Biosci. Biotechnol. Biochem. 76, 1296–1302. https://doi.org/10.1271/bbb.120050.

Radadiya, N., Parekh, V.B., Dobariya, B., Mahatma, L., Mahatma, M.K., 2016. Abiotic stresses alter expression of S-adenosylmethionine synthetase gene, polyamines and antioxidant activity in pigeon pea (*Cajanus cajan* L.). Legum. Res. 39. https://doi.org/10.18805/lr.v39i6.6640.

Rascio, N., Navari-Izzo, F., 2011. Heavy metal hyperaccumulating plants: how and why do they do it? And what makes them so interesting? Plant Sci. 180, 169–181. https://doi.org/10.1016/j.plantsci.2010.08.016.

Robinson, B., Lombi, E., Zhao, F., McGrath, S., 2003. Uptake and distribution of nickel and other metals in the hyperaccumulator *Berkheya coddii*. New Phytol. 158, 279–285. https://doi.org/10.1046/j.1469-8137.2003.00743.x.

Sakisaka, T., Meerlo, T., Matteson, J., Plutner, H., Balch, W.E., 2002. Rab-αGDI activity is regulated by a Hsp90 chaperone complex. EMBO J. 21, 6125–6135. https://doi.org/10.1093/emboj/cdf603.

Salt, D., Wagner, G., 1993. Cadmium transport across tonoplast of vesicles from oat roots. Plant Physiology. Amer Soc Plant Physiologists, p. 36.

Saminathan, T., Malkaram, S.A., Patel, D., Taylor, K., Hass, A., Nimmakayala, P., Huber, D.H., Reddy, U.K., 2015. Transcriptome analysis of invasive plants in response to mineral toxicity of reclaimed coal-mine soil in the Appalachian region. Environ. Sci. Technol. 49, 10320–10329. https://doi.org/10.1021/acs.est.5b01901.

Schuettpelz, E., Pryer, K.M., 2009. Evidence for a Cenozoic radiation of ferns in an angiosperm-dominated canopy. Proc. Natl. Acad. Sci. 106, 11200–11205. https://doi.org/10.1073/pnas.0811136106.

Schutzendubel, A., Polle, A., 2002. Plant responses to abiotic stresses: heavy metal-induced oxidative stress and protection by mycorrhization. J. Exp. Bot. 53, 1351–1365. https://doi.org/10.1093/jexbot/53.372.1351.

Shi, H., Rojas, R., Bonifacino, J.S., Hurley, J.H., 2006. The retromer subunit Vps26 has an arrestin fold and binds Vps35 through its C-terminal domain. Nat. Struct. Mol. Biol. 13, 540. https://doi.org/10.1038/nsmb1103.

Smardon, A.M., Kane, P.M., 2007. RAVE is essential for the efficient assembly of the C subunit with the vacuolar H+-ATPase. J. Biol. Chem. 282, 26185–26194. https://doi.org/10.1074/jbc.M703627200.

Südhof, T.C., Rothman, J.E., 2009. Membrane fusion: grappling with SNARE and SM proteins. Science 323, 474–477. https://doi.org/10.1126/science.1161748.

Takahashi, R., Bashir, K., Ishimaru, Y., Nishizawa, N.K., Nakanishi, H., 2012. The role of heavy-metal ATPases, HMAs, in zinc and cadmium transport in rice. Plant Signal. Behav. 7, 1605–1607. https://doi.org/10.4161/psb.22454.

Thomas, D., Cherest, H., Surdin-Kerjan, Y., 1991. Identification of the structural gene for glucose-6-phosphate dehydrogenase in yeast. Inactivation leads to a nutritional requirement for organic sulfur. EMBO J. 10, 547–553. https://doi.org/10.1002/j.1460-2075.1991.tb07981.x.

Thomas, P.D., Campbell, M.J., Kejariwal, A., Mi, H., Karlak, B., Daverman, R., Diemer, K., Muruganujan, A., Narechania, A., 2003. PANTHER: a library of protein families and subfamilies indexed by function. Genome Res. 13, 2129–2141. https://doi.org/10.1101/gr.772403.

Tkalec, M., Prebeg, T., Roje, V., Pevalek-Kozlina, B., Ljubešić, N., 2008. Cadmium-induced responses in duckweed *Lemna minor* L. Acta Physiol. Plant. 30, 881–890. https://doi.org/10.1007/s11738-008-0194-y.

van de Mortel, J.E., Schat, H., Moerland, P.D., van Themaat, E.V.L., Van Der Ent, S., Blankestijn, H., Ghandilyan, A., Tsiatsiani, S., AARTS, M.G., 2008. Expression differences for genes involved in lignin, glutathione and sulphate metabolism in response to cadmium in *Arabidopsis thaliana* and the related Zn/Cd-hyperaccumulator *Thlaspi caerulescens*. Plant Cell Environ. 31, 301–324. https://doi.org/10.1111/j.1365-3040.2007.01764.x.

Verbruggen, N., Hermans, C., Schat, H., 2009a. Mechanisms to cope with arsenic or cadmium excess in plants. Curr. Opin. Plant Biol. 12, 364–372. https://doi.org/10.1016/j.pbi.2009.05.001.

Verbruggen, N., Hermans, C., Schat, H., 2009b. Molecular mechanisms of metal hyperaccumulation in plants. New Phytol. 181, 759–776. https://doi.org/10.1111/j.1469-8137.2008.02748.x.

Walter, W., Sánchez-Cabo, F., Ricote, M., 2015. GOplot: an R package for visually combining expression data with functional analysis. Bioinformatics 31, 2912–2914. https://doi.org/10.1093/bioinformatics/btv300.

Werck-Reichhart, D., Feyereisen, R., 2000. Cytochromes P450: a success story. Genome Biol. 1, reviews3003. https://doi.org/10.1186/gb-2000-1-6-reviews3003.

WHO, 2010. Exposure to Cadmium: A Major Public Health Concern. World Health Organization, Geneva, Switzerland www.who.int/ipcs/features/cadmium.pdf, Accessed date: 1 June 2017.

Yoshihara, T., Tsunokawa, K., Miyano, Y., Arashima, Y., Hodoshima, H., Shoji, K., Shimada, H., Goto, F., 2005. Induction of callus from a metal hypertolerant fern, *Athyrium yokoscense*, and evaluation of its cadmium tolerance and accumulation capacity. Plant Cell Rep. 23, 579–585. https://doi.org/10.1007/s00299-004-0877-9.

Zhang, C.-H., Wu, Z.-Y., Ting, J., Ying, G., 2013. Purification and identification of glutathione S-transferase in rice root under cadmium stress. Rice Sci. 20, 173–178. https://doi.org/10.1016/S1672-6308(13)60114-6.

Zhang, B., Karnik, R., Waghmare, S., Donald, N., Blatt, M.R., 2017a. VAMP721 conformations unmask an extended motif for K+ channel binding and gating control. Plant Physiol. 173, 536–551. https://doi.org/10.1104/pp.16.01549.

Zhang, L., Zhao, H.-Y., Qi, W.-C., Zheng, F.-X., Wang, T.-Q., Li, J.-Y., 2017b. The analysis of mutant phenotypes and tissue expression reveals a role of SNAREs VAMP721 and VAMP722 in seedling growth. Biol. Plant. 61, 275–283. https://doi.org/10.1007/s10535-017-0745-4.